Reversible Host–Guest Crosslinks in Supramolecular Hydrogels for On-Demand Mechanical Stimulation of Human Mesenchymal Stem Cells

Philipp Linke, Natalie Munding, Esther Kimmle, Stefan Kaufmann, Kentaro Hayashi, Masaki Nakahata, Yoshinori Takashima, Masaki Sano, Martin Bastmeyer, Thomas Holstein, Sascha Dietrich, Carsten Müller-Tidow, Akira Harada, Anthony D. Ho, and Motomu Tanaka*

Stem cells are regulated not only by biochemical signals but also by biophysical properties of extracellular matrix (ECM). The ECM is constantly monitored and remodeled because the fate of stem cells can be misdirected when the mechanical interaction between cells and ECM is imbalanced. A well-defined ECM model for bone marrow-derived human mesenchymal stem cells (hMSCs) based on supramolecular hydrogels containing reversible host–guest crosslinks is fabricated. The stiffness (Young's modulus E) of the hydrogels can be switched reversibly by altering the concentration of non-cytotoxic, free guest molecules dissolved in the culture medium. Fine-adjustment of substrate stiffness enables the authors to determine the critical stiffness level E^* at which hMSCs turn the mechano-sensory machinery on or off. Next, the substrate stiffness across E^* is switched and the dynamic adaptation characteristics such as morphology, traction force, and YAP/TAZ signaling of hMSCs are monitored. These data demonstrate the instantaneous switching of traction force, which is followed by YAP/TAZ signaling and morphological adaptation. Periodical switching of the substrate stiffness across E^* proves that frequent applications of mechanical stimuli drastically suppress hMSC proliferation. Mechanical stimulation across E^* level using dynamic hydrogels is a promising strategy for the on-demand control of hMSC transcription and proliferation.

1. Introduction

The extracellular matrix (ECM) is a crucial component in maintaining the structural integrity and functionality of cells, as well as regulating the homeostasis of animal tissues.[1] Remodeling of ECM plays a significant role in regulating not only the behavior of single cells but also the morphogenesis of tissues.[2] Cells respond not only to extrinsic biochemical signals, such as gradients of chemokines or growth factors, but also to the biophysical cues from their surrounding microenvironment, including the topography and stiffness of the ECM. The adhesion, morphology, and migration of cells are influenced by the bulk Young's modulus of ECM model substrates when one uses chemically crosslinked hydrogels functionalized with ECM proteins.[3] Myoblasts differentiate into myotubes with pronounced actomyosin striation when cultured on hydrogel substrates possessing a Young's modulus similar to that of the native ECM.[4] The Young's modulus values of hydrogel substrates influence the

P. Linke, N. Munding, E. Kimmle, S. Kaufmann, M. Tanaka
Physical Chemistry of Biosystems
Institute of Physical Chemistry
Heidelberg University
69120 Heidelberg, Germany
E-mail: tanaka@uni-heidelberg.de

K. Hayashi, M. Bastmeyer, T. Holstein, A. D. Ho, M. Tanaka
Center for Integrative Medicine and Physics
Institute for Advanced Study
Kyoto University
Kyoto 606-8501, Japan

M. Nakahata, Y. Takashima
Department of Macromolecular Science
Graduate School of Science
Osaka University
Osaka 560-0043, Japan

M. Sano
Institute of Natural Sciences
Shanghai Jiao Tong University
Shanghai 200240, China

maintenance, self-renewal, and lineage-specific differentiation of somatic human mesenchymal stem cells (hMSCs).[5] Moreover, Weaver et al. reported that pluripotent human embryonic stem cells (hESCs) respond to the elasticity of hydrogel substrates. When the Young's modulus of the substrate is close to that of the ECM in vivo, hESCs undergo β-catenin/Wnt-dependent mesoderm differentiation.[6] However, an imbalance in the mechanical interaction between cells and their microenvironment can mislead the fate of stem cells. The violation of mechanical compliance can cause severe problems when transplanting stem cells to damaged or diseased tissues, as distinct differences in ECM stiffness can result in undefined lineages. For example, injecting hMSCs intravenously into a fibrotic liver causes them to differentiate into ductal cells instead of becoming hepatocytes, as the fibrotic liver is stiffer than a healthy liver.[7]

The stiffness of microenvironments is sensed by the dynamic mechanical junctions composed of integrin receptors connected to the actomyosin complex via adaptor proteins. These focal adhesions act as molecular "clutches" and transmit mechanical information to downstream signaling pathways.[8] Adaptor proteins, such as talin and vinculin, connect integrin receptors and actomyosin complexes, generating traction forces. Notably, these proteins form an inactive complex in the cytoplasm but get activated only when recruited to focal adhesions. When a force is exerted on talin, it unfolds its helical bundles to expose cryptic binding domains that facilitate its activation. The availability of binding sites for other focal adhesion proteins is modulated by the stepwise unfolding of each helical bundle in response to the forces generated by the actomyosin complex, leading to the recruitment

of vinculin. Elosegui-Artola et al. showed that substrate stiffness, matrix density, and myosin contractility modulate the threshold level, which can be explained within the framework of a strain-dependent "molecular clutch" model.[8c] Beyond this threshold, the binding of vinculin to unfolded talin leads to focal adhesion growth, resulting in the transfer of the transcriptional factor YAP/TAZ to the cell nucleus.[9]

YAP/TAZ proteins are transcription factors that migrate between the cytoplasm and cell nucleus. They are regulated by various input signals, including those from the Hippo pathway.[10] In the nucleus, YAP/TAZ complexes with TEA domain transcription factors to upregulate various genes responsible for different cellular functions such as proliferation, stress resistance, and organ overgrowth.[11] The level of YAP/TAZ activity is tightly linked to various biomechanical inputs, including cell–ECM and cell–cell contacts.[10] YAP/TAZ activity are modulated not only by biochemical perturbations of focal adhesion and cytoskeletons, as shown by the knockdown of vinculin[12] and inhibition of Rho GTPase,[11c] but also by biomechanical cues, such as the reduction of cell–substrate contact area and substrate stiffness.[11c] Therefore, high traction forces from large adhesion contacts or stiff substrates can induce nuclear localization of YAP/TAZ.[13] The influence of substrate stiffness on YAP/TAZ activity have been studied using chemically crosslinked polyacrylamide gels. Dupont et al. observed pronounced nuclear localization of YAP/TAZ in hMSCs on gels with Young's modulus $E = 40$ kPa but not on gels with $E = 0.7$ kPa.[11c] Kuroda et al. also reported a monotonic increase in the nuclear localization of YAP/TAZ in mouse MSCs with increasing elasticity but were unable to identify a clear threshold level.[9] A distinct increase in nuclear YAP/TAZ levels in mouse embryonic fibroblasts was found between $E = 5$ and 10 kPa,[8c] but the critical substrate stiffness that turns on/off the mechanosensing of hMSCs has not been determined. Moreover, despite the highly dynamic nature of mechano-sensory machinery in cells, these previous studies used chemically crosslinked hydrogels with fixed elasticity levels. Although there have been several studies shedding light on the dynamic stiffening and softening of matrix on hMSCs,[14] the quantitative understanding on the dynamic response of mechano-sensory machines to an abrupt change in substrate stiffness is largely missing.

In this study, we conducted a quantitative investigation into the dynamic response of hMSCs to abrupt changes in their surrounding environments at critical stiffness levels that activate or deactivate their mechano-sensory machinery both in situ and ex situ. In a dynamic hMSC ECM model, we employed supramolecular hydrogels that contain reversible host–guest crosslinks.[15] Their bulk Young's modulus can be altered on-demand by adding or removing free host or guest molecules through competitive binding and unbinding of free host or guest molecules to pre-formed host–guest inclusion complexes, unlike the Young's modulus of the commonly used, chemically crosslinked hydrogels.[16] In this study, we fabricated polyacrylamide hydrogels with β-cyclodextrin (host) and adamantane (guest) moieties as side chains and functionalized the hydrogel surface with fibronectin. First, we determined the critical stiffness level at which hMSCs activate or deactivate the mechano-sensory machinery ($E^* \approx 20$ kPa) by screening the bulk Young's modulus of hydrogels over a wide range. Second, we investigated the

M. Bastmeyer
Cell and Neurobiology
Zoological Institute
Karlsruhe Institute of Technology
76131 Karlsruhe, Germany

M. Bastmeyer
Institute for Biological and Chemical Systems – Biological Information Processing (IBCS-BIP)
Karlsruhe Institute of Technology
76334 Eggenstein-Leopoldshafen, Germany

T. Holstein
Molecular Genetics and Evolution
Centre for Organismal Studies
Heidelberg University
69221 Heidelberg, Germany

S. Dietrich, C. Müller-Tidow, A. D. Ho
Department of Internal Medicine V
Hematology, Oncology, Rheumatology
University Hospital Heidelberg
69120 Heidelberg, Germany

S. Dietrich
Department of Haematology, Oncology, and Clinical Immunology
Universitätsklinikum Düsseldorf
40225 Düsseldorf, Germany

A. Harada
The Institute of Scientific and Industrial Research
Osaka University
8-1 Mihogaoka, Ibaraki, Osaka 567-0047, Japan

A. D. Ho
Molecular Medicine Partnership Unit Heidelberg
EMBL and Heidelberg University
69120 Heidelberg, Germany

**ADVANCED
SCIENCE NEWS**

www.advancedsciencenews.com

**ADVANCED
HEALTHCARE
MATERIALS**

www.advhealthmat.de
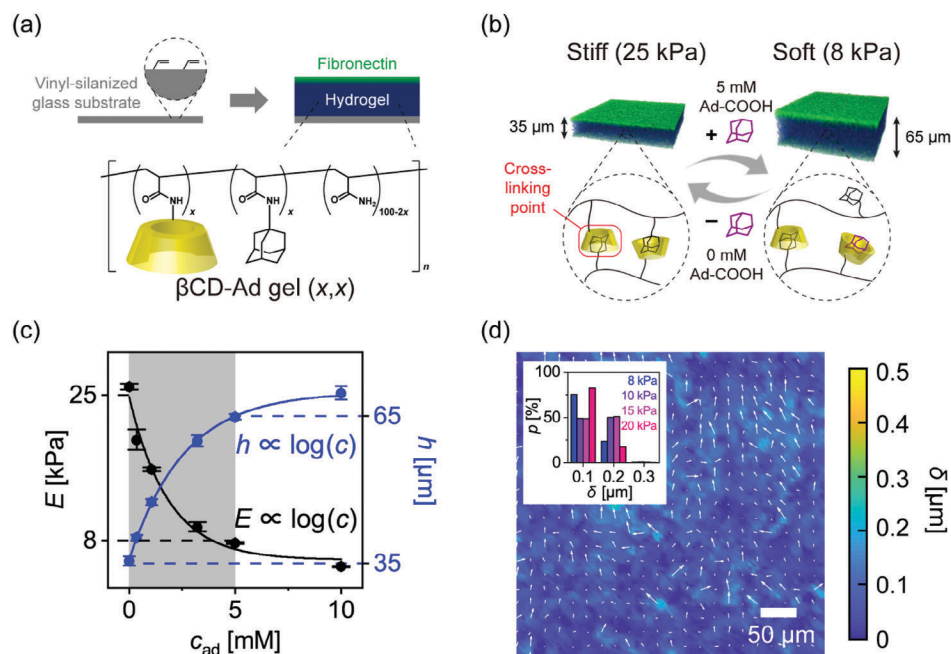
Figure 1. Supramolecular hydrogel (βCD–Ad gel) crosslinked by reversible host–guest interactions. a) Schematic illustration and chemical structure of a supramolecular hydrogel (β-cyclodextrin [βCD]–adamantane [Ad] gel [x,x]) on the vinyl-silanized glass substrate. The hydrogel surface was functionalized with fibronectin for the stable cell adhesion. b) Oblique views of the supramolecular hydrogel coated with Alexa Fluor 488-labeled fibronectin (green), switching the bulk elastic modulus E and thickness h. Initially, polyacrylamide chains are crosslinked via inclusion complexes of βCD and Ad. In the absence of soluble guest molecules, the thickness and bulk elastic modulus of βCD–Ad gel (3,3) presented in the figure are $h = 35$ μm and $E = 25$ kPa, respectively. The addition of 5 mM adamantane carboxylic acid (Ad-COONa) led to a decrease in the number of crosslinking points, resulting in the increase of h to 65 μm and decrease of E to 8 kPa. Conversely, both h and E can be switched back to the initial level by the depletion of Ad-COONa from the medium. c) E and h plotted as a function of [Ad-COONa]. Note that both E and h are switchable with no hysteresis by changing [Ad-COONa] in the medium. d) The lateral displacement δ of fluorescent beads embedded near the surface after incubation with 5 mM Ad-COONa for 10 min. The magnitude of displacement is indicated by the color code, while the direction is indicated by the white arrows. The inset shows the distribution of bead displacements caused by softening the gels from 25 to 20, 15, 10, and 8 kPa. More than 99% of the beads showed the lateral displacement of $\delta \leq 0.2$ μm, confirming that the gel swells only in the direction perpendicular to the surface.

dynamic response of hMSCs in response to the change in Young's modulus from 25 to 15 kPa. We monitored the morphology, active traction force, and YAP/TAZ translocation over time. Our data demonstrate that abrupt substrate softening turns off the traction force instantaneously even before the hMSCs change shape by disassembling focal adhesions and remodeling actin cytoskeletons. Moreover, the morphological adaptation and delocalization of YAP/TAZ occurred simultaneously, suggesting that both processes are downstream of mechanical forces. Finally, we found that periodic changes in substrate stiffness across E^* values suppressed the proliferation of hMSCs, suggesting that hMSCs escape from the normal cell cycle under frequent stress. The supramolecular hydrogel substrates used in this study have significant potential for gaining deeper insights into static and dynamic mechanosensing by various cells as well as for on-demand extrinsic modulation of gene expression and stem cell proliferation.

2. Results

2.1. Switching Young's Modulus of Supramolecular Hydrogels

Figure 1a shows schematic illustration and chemical structure of the hydrogel (βCD–Ad gel (x,x)) used in this study. Acrylamide

(AAm) was copolymerized with 6-acrylamido-βCD (βCD–AAm, x mol%) and adamantane-acrylamide (Ad–AAm, x mol%) on the glass substrate coated with a vinylsilane monolayer. The resulting hydrogel is crosslinked via non-covalent, host–guest interaction of βCD and Ad moieties. The hydrogel surface was functionalized with fibronectin via bifunctional Sulfo-SANPAH crosslinker, because hMSCs do not adhere to as-prepared βCD–Ad gels with no surface functionality (Figure S1, Supporting Information).[15b] Figure 1b shows oblique views of the host–guest hydrogel (βCD–Ad gel (3,3)) reconstructed from confocal microscopy images in the absence (left) and presence (right) of [Ad-COONa] = 5 mM. The surface level was visualized by fibronectin labeled with Alexa Fluor 488 (green). As illustrated in the figure, the polymer chains are crosslinked by stable inclusion complexes of host–guest moieties at [Ad-COONa] = 0 mM, forming a compact ($h \approx 35$ μm) but stiff hydrogel with a high bulk elastic modulus, $E \approx 25$ kPa. When free Ad-COONa was added to the medium, Ad-COONa in solution started competing with the Ad moieties connected to the polymer chain. Because the number of available host βCD moieties was limited, some of the βCD–Ad inclusion complexes dissociated due to the shift in chemical equilibrium. Subsequently, a decrease in the density of crosslinks in polymer networks led to an increase in thickness ($h \approx 65$ μm) and a decrease in bulk elastic modulus, $E \approx 8$ kPa. Conversely, exchanging the medium

with a medium containing no Ad-COONa led to the dissociation of βCD-Ad-COONa complexes, resulting in the recovery of the original thickness and elastic modulus, $h \approx 35$ μm and $E \approx 25$ kPa, respectively. As the Young's modulus E and equilibrium thickness h of host–guest hydrogels are important physico-chemical parameters in mechanical control of hMSCs, Figure 1c depicts the plot of these two values as a function of [Ad-COONa] in the medium. Both E and h were proportional to log[Ad-COONa] (solid line), reflecting the equilibrium between the chemical potential of Ad-COONa in solution and that in hydrogel. The kinetics of the change in E was monitored by in situ AFM indentation under a constant flow of 1 mL min^{-1}, indicating that the softening occurs in ≈ 30 min and the stiffening takes about 1 h (Figure S2, Supporting Information). Because the medium exchange was not continuous during the experiments with hMSC, we also monitored the change in E after the medium exchange (ex situ AFM indentation, Figure S3, Supporting Information). The softening required only one medium exchange to the medium with Ad-COONa, and the E value was stable in 10 min. On the other hand, it was necessary to exchange the medium three times to stiffen the gel to the original level. Taking time for the medium exchange and the incubation per one cycle (1 h), we counted 3 h for the stiffening of the gel. Figure 1d represents the lateral displacement of embedded fluorescent beads caused by the addition of 5 mM Ad-COONa, tracked by particle image velocimetry (PIV). The color code indicates the magnitude, and the arrow indicates the direction of lateral displacement. Although the change in thickness was in tens of μm, the lateral displacement δ of more than 99% of the beads was ≤ 0.2 μm (inset). This finding confirms that the swelling of supramolecular gels occurs only in the direction perpendicular to the surface and not parallel to it. The anisotropic swelling of supramolecular hydrogels is explained by the physical constraint due to the covalent anchoring of the bottom to the solid substrates.[17] Notably, the use of non-covalent supramolecular crosslinks enables the fine adjustment of elastic modulus E in a reversible manner and the dynamic changes in elasticity on exchange of the culture medium (Figures S2 and S3, Supporting Information).

2.2. Morphological Patterns of hMSCs as a Function of Bulk Young's Modulus

Figure 2a,e shows representative phase contrast microscopy images and the aspect ratio (AR) plotted versus projected cell area (A_{proj}) of hMSCs on supramolecular hydrogels with $E = 8$, 10, 15, 20, and 25 kPa, corresponding to [Ad-COONa] = 5, 3.2, 1.1, 0.36, and 0 mM, respectively. For comparison, Figure 2f shows the corresponding morphometric map acquired on fibronectin-coated glass. Prior to the experiments, we confirmed that [Ad-COONa] levels from 0–5 mM do not influence hMSC viability (Figure S4, Supporting Information). AR represents the axial elongation, while A_{proj} represents the spreading. Instead of discussing about AR or A_{proj} individually, 2D maps (AR vs A_{proj}) were used to extract the characteristic morphological patterns as a function of E because these two parameters showed different distributions on soft and stiff substrates, as described below. As presented in Figure 2a,b, the distribution of projected area of hMSCs remained within a narrow range ($A_{proj} < 2500$ μm^2) on soft

hydrogel substrates ($E = 8$ and 10 kPa), while the aspect ratio exhibited a more pronounced scatter. This suggests that the cells are free to take any shape due to no restriction but keep the contact are to hydrogel small. At $E = 15$ kPa (Figure 2c), the characteristic patterns of morphology started changing, and hMSCs exhibited a distinctly different morphological pattern that can be characterized by a smaller aspect ratio (AR < 10) with a widely distributed A_{proj} on substrates at $E = 20$ and 25 kPa (Figure 2d,e). This suggests that hMSCs on stiff gels spread not only axial direction but also in transverse direction, but the degree of spreading (A_{proj}) is widely distributed. Of note, the morphological patterns at $E = 20$ and 25 kPa (Figure 2e) were nearly indistinguishable from those at $E \approx 1$ GPa (glass substrates, Figure 2f). By screening the bulk Young's modulus over a wider range beyond the physiological level ($E = 80–400$ kPa, Figure S5, Supporting Information), we confirmed that hMSCs cannot discriminate higher values ($E \geq 20$ kPa). These data suggest that the morphological adaptation of hMSCs is triggered at $E \approx 20$ kPa, but they are no longer able to discriminate the stiffer matrix environments above this level.

2.3. Substrate Stiffness Modulates Focal Adhesion and Actin Cytoskeleton

In the next step, we investigated the influence of substrate stiffness on the spatial distribution of focal adhesions and the arrangement of actin cytoskeletons at the sub-cellular level, which govern the morphological adaptation of cells. Actin cytoskeletons are connected to integrin clusters via adaptor proteins like talin and vinculin and generate forces. As shown by Zemel et al.,[18] the orientational alignment of actin stress fibers, characterized by the nematic order parameter, play key roles in the mechanical coupling between substrates and cells.

Focal adhesions were detected by immuno-fluorescence staining of activated vinculin, which undergoes a conformational change from closed (inactive) to open (active) form upon contact with a stiff matrix.[19] To visualize the active vinculin that binds to actin filaments, hMSCs were pre-treated with cytoskeletal buffer (CSK buffer),[20] which removed all inactive vinculin molecules in the cytoplasm before staining. **Figure 3a** shows the immunocytochemical image of focal adhesions (vinculin, green) and nucleus (DAPI, blue) on stiff (25 kPa) substrates. The higher magnification images (insets) indicate the accumulation of stable, elongated focal adhesion complexes near the cell periphery. Following the protocol presented in Figure S6 (Supporting Information), we calculated the total area of focal adhesions per cell. As shown in Figure 3b, the total area of focal adhesions on stiff gels ($E = 20$ and 25 kPa) is significantly larger than that on soft gels (8 kPa, $p = 0.015$), which agrees well with previous findings on mouse mesenchymal stem cells.[12,21]

Figure 3c shows the binarized immunocytochemical image of actin cytoskeletons, following the protocol shown in Figure S7 (Supporting Information). The actin filaments were binarized by intensity thresholding, and the major axis of the best fitting ellipse (broken line) defines $\theta = 0°$ (white arrow). The color code corresponds to the angle between each actin filament and the major axis of the cell θ. The directional ordering of actin cytoskeletons was assessed by calculating the nematic order parameter

**ADVANCED
SCIENCE NEWS**

www.advancedsciencenews.com

**ADVANCED
HEALTHCARE
MATERIALS**

www.advhealthmat.de
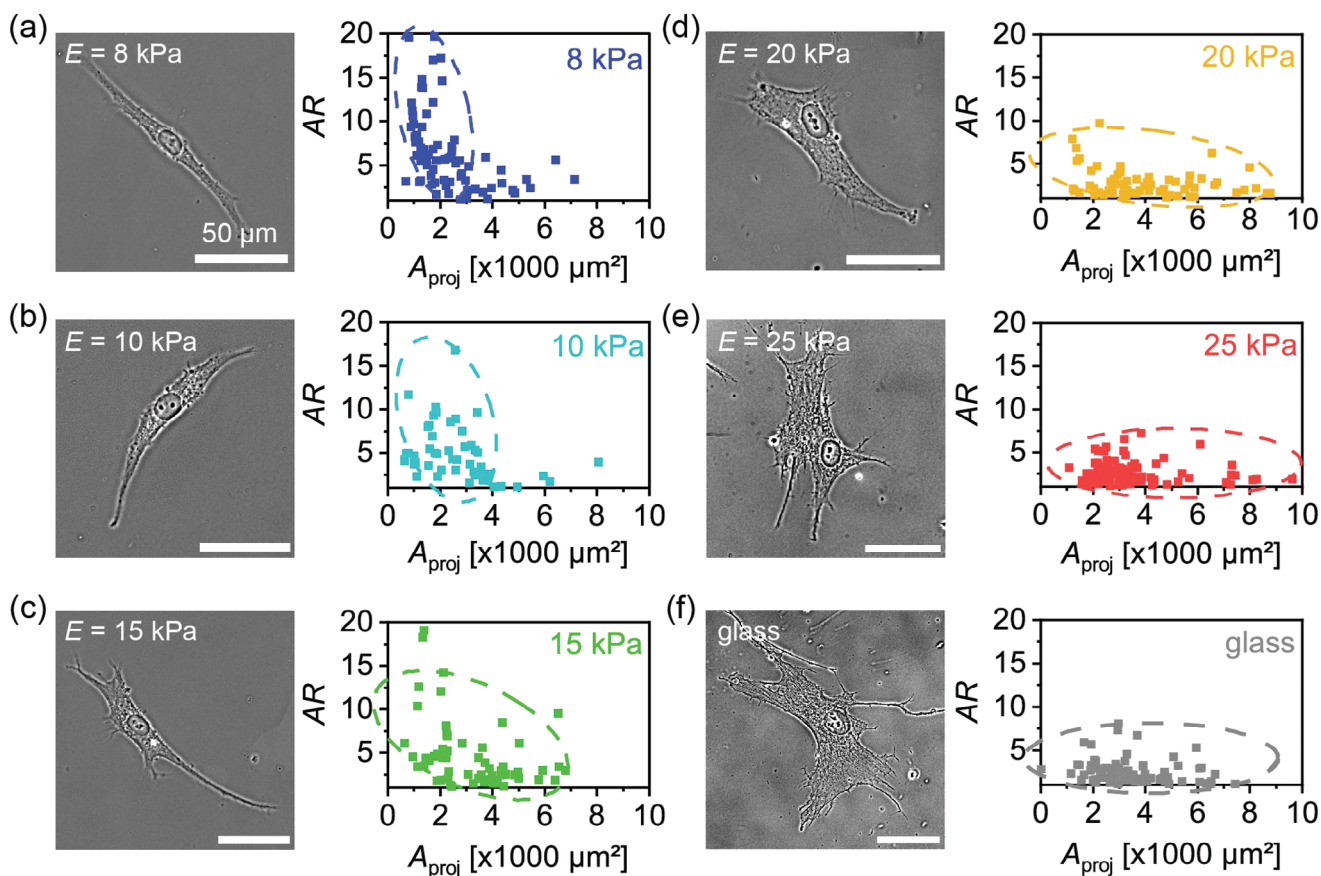
Figure 2. Morphometric patterns of human mesenchymal stem cells (hMSCs) versus Young's modulus. Phase contrast images (left) and morphometric maps (right) of hMSCs on supramolecular hydrogel substrates in the presence of a) [Ad-COONa] = 5 mM (E = 8 kPa), b) 3.2 mM (10 kPa), c) 1.1 mM (15 kPa), d) 0.36 mM (20 kPa), and e) 0 mM (25 kPa). For comparison, the corresponding data taken on fibronectin-coated glass are shown in panel (f). Each dataset consists of data from $N \geq 54$ cells. Morphological maps, represented by aspect ratio (AR) versus projected area (A_{proj}), are almost indistinguishable between E = 20 kPa and at $E \approx 1$ GPa, suggesting that the mechanosensing of hMSCs does not discriminate the substrate stiffness beyond 20 kPa.

$\langle S \rangle$ weighted by the area of each filament following Equation (1) (Figure S8, Supporting Information)[18,22]

$$\langle S \rangle = \frac{\sum_i A_i \cdot \cos(2\theta_i)}{\sum_i A_i} \tag{1}$$

A_i is the pixel number multiplied by the corresponding fluorescence intensity of the i-th filament, which reflects the length and thickness of each filament. This takes the length and thickness of actin filaments into account.[22c] As summarized in Figure 3d, the median values of order parameters calculated from more than 20 cells showed the difference in actin ordering between stiff (0.56) and soft substrates (0.80) is statistically significant ($p < 0.05$).

2.4. Active Traction Force Increases at $E^* > 20$ kPa

Phosphoinositide 3-kinase is activated by binding to focal adhesion and phosphorylates phosphatidylinositol (4,5)-bisphosphate. This initiates the logistic recruitment of key proteins required for remodeling the actin cytoskeleton and hence

generates traction forces in the extracellular environment.[23] To quantitatively determine the spatial pattern of forces generated by hMSCs, we monitored the displacement of 0.2 μm-large fluorescent beads embedded in the vicinity of substrate surfaces (**Figure 4a**) and calculated the spatial distribution of traction stress.[24] Figure 4b represents a typical traction stress field and the corresponding force dipoles M_{ij} (Equation (2))

$$M_{ij} = \int r_i T_j \mathrm{d}x\mathrm{d}y \tag{2}$$

where r_i and T_j are the position and traction forces of the ith and jth components, respectively. The dipole matrix is symmetric and hence diagonalized because the net moment of inertia of the system is negligible.[25] This enables the calculation of major and minor eigenvectors possessing larger and smaller eigenvalues, D_{max} and D_{min}, respectively. The directions of the eigenvectors are indicated by white arrows, while their magnitudes are shown by the length of the arrows. The inset is a zoom-up of the traction stress field near the cell periphery (red), indicating that the large traction stresses pointing toward the cell center correspond to the contraction of actomyosin complexes.

**ADVANCED
SCIENCE NEWS**

www.advancedsciencenews.com

**ADVANCED
HEALTHCARE
MATERIALS**

www.advhealthmat.de
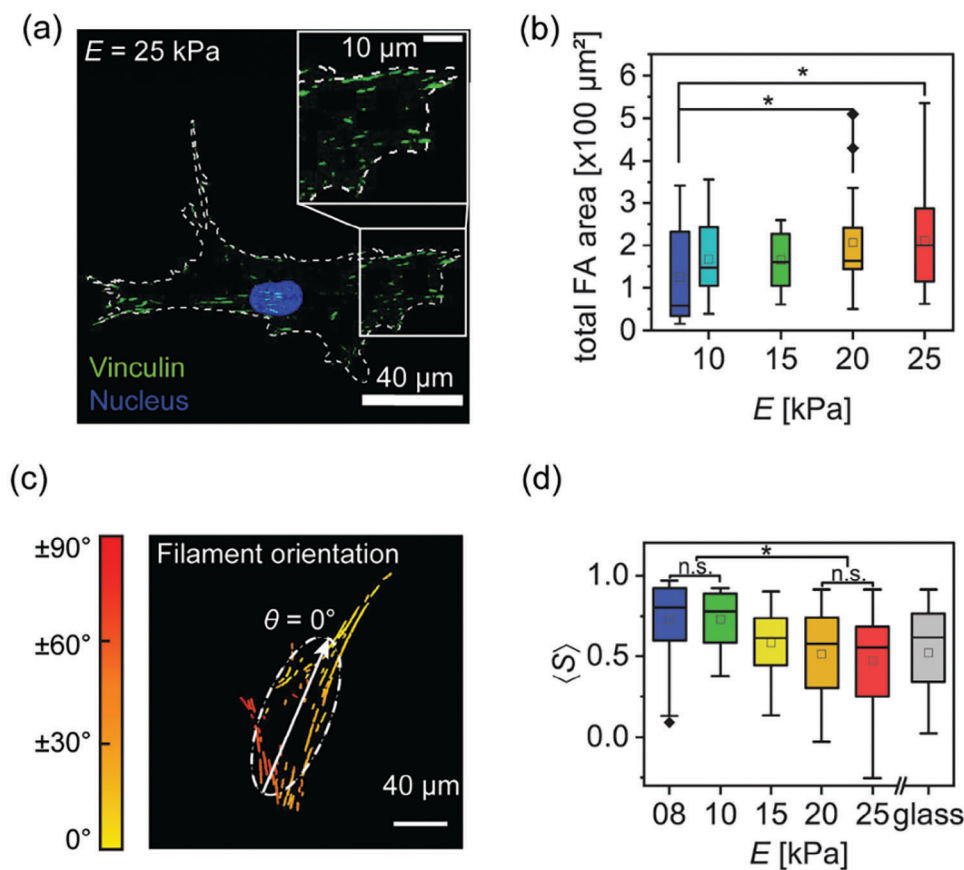
Figure 3. Substrate stiffness modulates focal adhesion and actin cytoskeleton. Immunocytochemical image of hMSC on stiff gel ($E = 25$ kPa). Green; vinculin, blue; cell nucleus. b) Total focal adhesion area per cell plotted versus E. The asterisk indicates a significant difference with p-value < 0.05 by Student's t-test. c) Binarized immunocytochemical image of actin cytoskeletons. The color code corresponds to the angle between each actin filament and the major axis of the cell θ, where $\theta = 0°$ (white arrow) is defined from the best fitting ellipse (broken line). d) Nematic order parameter $\langle S \rangle$ weighted by the area of each filament plotted versus E. The asterisk indicates a significant difference ($p < 0.05$ by Student's t-test).

From the traction force $\vec{T}(\vec{r})$ and the particle displacement $\vec{u}(\vec{r})$, one can calculate the total strain energy with Equation (3)[26]

$$U = \frac{1}{2} \int \vec{T}(\vec{r}) \, \vec{u}(\vec{r}) \, \mathrm{d}x \, \mathrm{d}y \tag{3}$$

which reflects the energy transferred from the cell to the substrate by elastic deformation. Here, we directly integrated the strain energy density inside the region of interest instead of Fourier analyses to avoid possible artifacts at the field boundary. As presented in Figure S9 (Supporting Information), the total strain energy U exhibited a monotonic increase with increasing substrate elasticity. Net contractile moment μ can be obtained by the trace of diagonalized dipole matrix[26a–c]

$$\mu = tr \begin{pmatrix} D_{\min} & 0 \\ 0 & D_{\max} \end{pmatrix} \tag{4}$$

μ only takes the strains in the direction of the principal axis of traction into account, while excluding rotation in cells. It should be noted that U and μ are distinctly different from their physical definitions, although both are given in the same unit [J]. U represents an energy calculated by force times displacement, while

μ a moment calculated by force times distance from the origin. As presented in Figure 4c, μ increased from 1 to 5 nJ with an increase in substrate stiffness from 8 to 25 kPa. The transition of μ is accompanied by the increase in AR that reflects the axial stretch of the cell body, which is characterized by AR. This seems reasonable, because μ per se represents the traction force parallel to the direction of cell elongation. In fact, the plot of μ versus AR (Figure 4d) indicates two distinct patterns corresponding to $E = 8$ and 10 kPa (blue ellipse) and $E = 25$ kPa (red ellipse). On the other hand, the μ–AR patterns for hydrogels with the Young's modulus of $E = 10$–20 kPa can be categorized into one group (black ellipse), suggesting that this regime is the intermediate state between soft (blue) and stiff (red) patterns.

2.5. Cell Adhesion Strength Increases at $E^* > 20$ kPa

The transition of morphological patterns, the spatial arrangement of focal adhesion and actin cytoskeleton, and the traction force generation could be attributed to the manifestation of mechanical interactions between hMSCs and hydrogel substrates. To gain more insight into the mechanical coupling of hMSCs and hydrogel substrates, we used our self-built setup to

2302607 (6 of 17)

**ADVANCED
SCIENCE NEWS**

www.advancedsciencenews.com

**ADVANCED
HEALTHCARE
MATERIALS**

www.advhealthmat.de
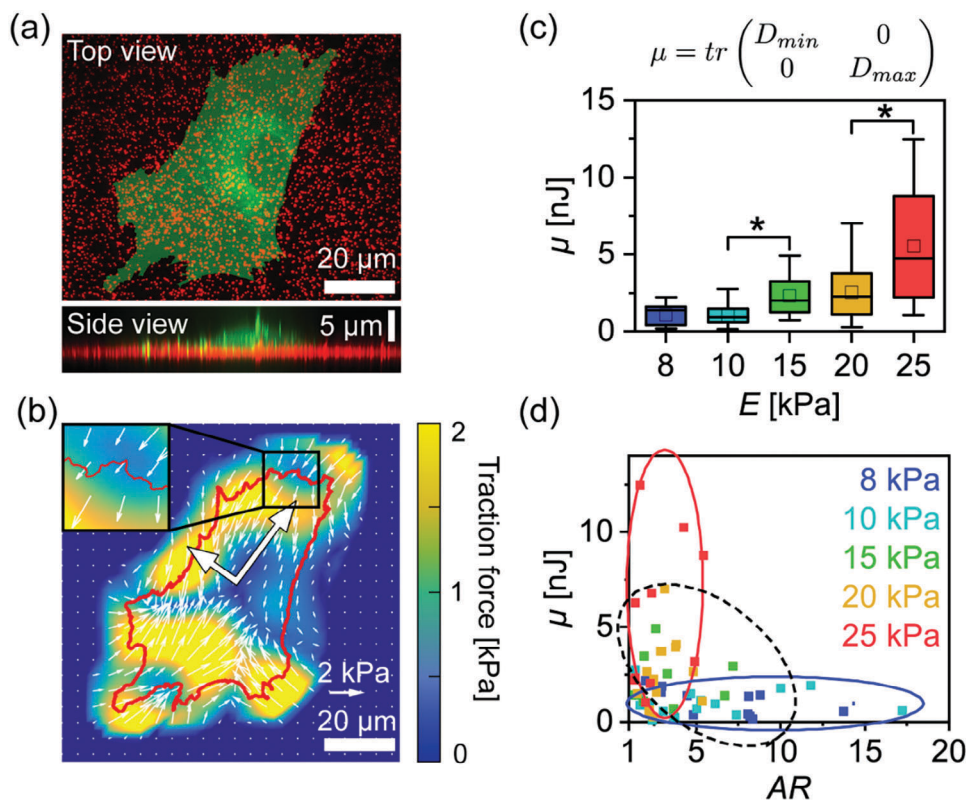
Figure 4. Adhesion-induced traction forces increases at $E^* > 20$ kPa. a) Top and side views of hMSCs on a supramolecular hydrogel substrate ($E =$ 25 kPa) embedding fluorescent beads (diameter: 0.2 µm). The cell membrane was labeled with CellBrite (green). The side view confirmed that the beads (red) are confined in the close vicinity of the surface. b) Traction stress field and the corresponding force dipoles extracted from hMSC on a substrate with $E =$ 25 kPa. Red line highlights the cell rim. White arrows show the direction of the traction force, while the length of arrows and the color represent the magnitudes. The eigenvectors of force dipoles (D_{max} and D_{min}) are shown by large white arrows. Inset shows the zoom-up image of force field near the cell periphery. c) Net contractile moment μ of hMSCs on substrates with different E. Each dataset consists of data from $N \geq 8$ cells. The asterisk indicates a significant difference with p-value < 0.05 by Student's t-test. d) μ was plotted as a function of aspect ratio AR of cells. The data corresponding to $E =$ 8 and 10 kPa are surrounded by a blue solid line, $E =$ 15 and 20 kPa by a black broken line, and $E =$ 25 kPa by a red solid line.

measure hMSC adhesion strength (**Figure 5a**).[22a,27] Our non-invasive method uses a laser pulse to induce a pressure wave, allowing us to determine the critical pressure required for cell detachment (see Figure S10, Supporting Information, for more detail).[27,28] Binarized microscopy images of hMSCs on a substrate with $E =$ 15 kPa before (left) and after (right) exposure to the pressure wave are shown in Figure 5b. The red broken line in the figure indicates the range within which the cavitation bubble could reach ($r \leq 0.5$ mm, Figure S11, Supporting Information), while the yellow ring indicates the region ($\Delta d =$ 100 µm) exposed to $P =$ 4.1 MPa. As shown in Figure 5c, the critical pressure P^* for cell detachment can be calculated by fitting the data with the error function (Equation (5))

$$\chi\ (P) = 1 - \frac{1}{2}\left(\text{erf}\left(\frac{P - P^*}{\sqrt{2}\sigma}\right) + 1\right) \tag{5}$$

where P^* is the critical pressure for cell detachment, and σ is the standard deviation. The transition points, indicated by black symbols, were defined as the point at which the first derivative $\delta\chi/\delta P$ takes the minimum. As shown in Figure 5d, the full width at half maximum (FWHM) of $\delta\chi/\delta P$ reflects the width of the transi-

tion, indicating the sharpening of the adhesion-detachment transition with increasing substrate elasticity. The observed tendency is summarized in Figure 5e, where P^* and FWHM are plotted as a function of E. Intriguingly, the transition pressure P^* exhibited a significant increase from $P^* =$ 4.2 MPa ($E =$ 20 kPa) to $P^* =$ 5.0 MPa ($E =$ 25 kPa) with $p < 0.001$, whereas the decrease in FWHM seemed more continuous with increasing E. These measurements were also carried out on chemically crosslinked gels, whose Young's modulus is beyond the physiological level ($E =$ 80–400 kPa). We found a monotonic increase in P^* with increasing E that reached the saturation ($P^* \approx 8$ MPa) when the Young's modulus was beyond 100 kPa (Figure S12, Supporting Information).

2.6. Nuclear Translocation of YAP/TAZ is Turned On at $E^* > 20$ kPa

The change in the traction force generation (Figure 4) and the mechanical strength of cell adhesion (Figure 5) strongly suggests that hMSCs turn on/off the mechano-sensory machinery at $E^* > 20$ kPa. To monitor the transduction of mechanical stimuli to the cell nucleus, we determined the spatial distribution
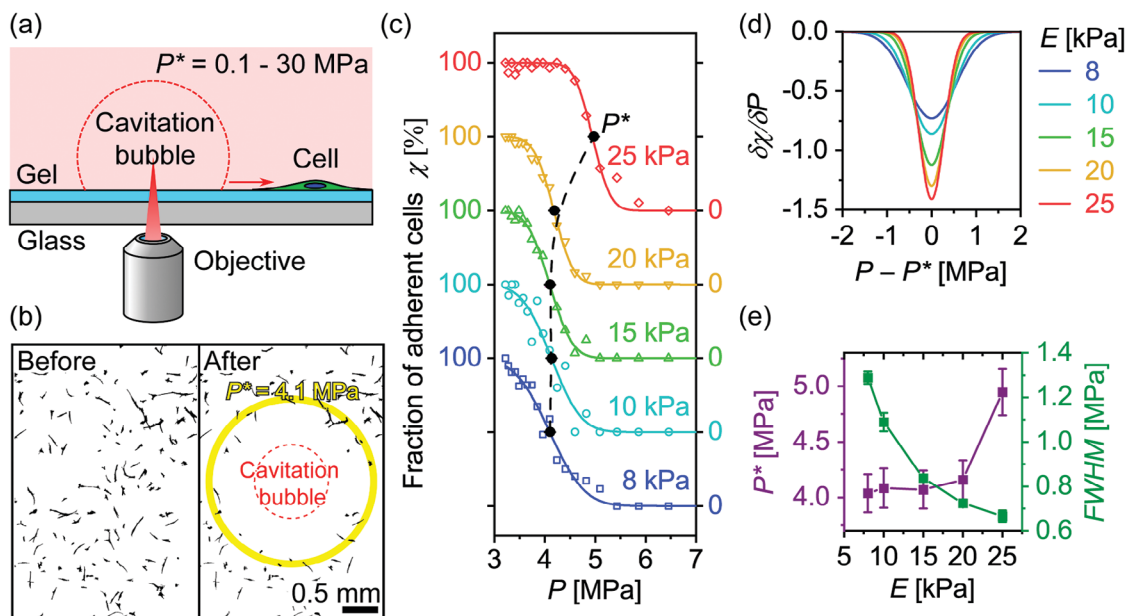
Figure 5. Cell adhesion strength increases at $E* > 20$ kPa. a) Quantification of cell adhesion strength using laser-induced pressure wave. b) Binarized images of cells on a hydrogel substrate ($E = 15$ kPa) before (left) and after (right) the irradiation with a laser pulse. Size of the cavitation bubble is indicated by a red broken line. The yellow belt corresponds to the region ($\Delta d = 100$ μm) exposed to $P = 4.1$ MPa. c) Fractions of adherent cells χ on substrates with different values of E, plotted as a function of pressure P. The data points were fitted with error function. The critical pressures corresponding to the binding–unbinding transition $P*$ are indicated by black circles, connected by a black broken line. d) Change in the width of binding–unbinding transition evaluated from $\delta\chi/\delta P$. To compare different data sets, P was converted to P–$P*$. e) Effect of substrate elasticity E on $P*$ and the width (FWHM) of $\delta\chi/\delta P$. $P*$ showed a significant increase from $P* = 4.2$ MPa ($E = 20$ kPa) to $P* = 5.0$ MPa ($E = 25$ kPa) with $p < 0.001$, while the decrease in $\delta\chi/\delta P$ was continuous with increasing E.

of YAP/TAZ proteins in the cytoplasm and the nucleus, following the previous reports.[29] The exact procedure is described in the Supporting Information (Figure S13, Supporting Information) and **Figure 6**a shows phase contrast (upper panels) and immunofluorescence images (lower panels) of hMSCs stained with YAP/TAZ antibodies on hydrogel substrates. As a reference, we presented the corresponding data on fibronectin-coated glass substrates. When Young's modulus was increased from $E = 10$, 15, 20, to 25 kPa, the anti-YAP/TAZ signals in the nuclei started getting more prominent. In Figure 6b,c, the ratios of anti-YAP/TAZ signals between the nucleus (Nuc) and the cytoplasm (Cyto), Nuc/Cyto, are plotted as a function of aspect ratio AR. Both the absolute Nuc/Cyto values and their distribution are in good agreement with those in previous report.[29b,c,30] As shown in Figure 5b,c, the plot of Nuc/Cyto versus AR suggested two distinct characteristic patterns. The hMSCs on soft hydrogels ($E = 8$–15 kPa) showed low Nuc/Cyto ratios (1.0–2.5) over a wide range of AR, suggesting that the explicit nuclear localization of YAP/TAZ is suppressed irrespective of the shape (Figure 6b). In contrast, the hMSCs on stiff hydrogels ($E = 20$ and 25 kPa) and glass substrates exhibited a large variation of Nuc/Cyto ratios (1.5–4.0) confined within AR < 10, which suggests the nuclear localization of YAP/TAZ in spread and hence contractile hMSCs (Figure 6c).

We further analyzed the degree of YAP/TAZ translocation more quantitatively by classifying the observed phenotypes into three categories (Figure 6d): i) comparable distribution in the nucleus and cytoplasm (Nuc/Cyto < 1.5, blue), ii) preferential nuclear localization (Nuc/Cyto = 1.5–2.5, red), and iii) explicit nuclear localization (Nuc/Cyto > 2.5, grey). Notably, the fraction of

cells showing explicit nuclear localization (Nuc/Cyto > 2.5, grey) increased from 4% ($E = 15$ kPa), 14.3% ($E = 20$ kPa), and to 36.1% ($E = 25$ kPa). As shown in Figure S14 (Supporting Information), the further increase in Young's modulus even beyond the physiological level (up to 400 kPa) led to a monotonic increase in the fraction of cells showing the explicit nuclear localization up to 65%. Previously, Dupont et al. restricted the size of the cell–substrate contact area by micro-contact printing of fibronectin on glass substrates and demonstrated that the YAP/TAZ nuclear localization decreased with decreasing contact area.[13] In fact, we found a positive correlation between the Nuc/Cyto ratio and projected cell area A_{proj} (Figure S15, Supporting Information), showing the same trend.

2.7. In Situ Monitoring of Traction Force in Response to Elasticity Jump Across $E*$

In contrast to widely used chemically crosslinked hydrogels, our supramolecular hydrogel is able to change its Young's modulus reversibly by simply altering the concentration of free host/guest molecules in the medium. This allows for the mechanical stimulation of cells with a defined ΔE on-demand, at the desired time point t and frequency f. As a proof of concept, we monitored the change in traction force of hMSCs in response to an abrupt softening of the substrate across the critical level, $E* \approx 20$ kPa.

To accomplish this, hMSCs were initially seeded on the hydrogel substrate without Ad-COONa ($E = 25$ kPa) and allowed to

**ADVANCED
SCIENCE NEWS**

www.advancedsciencenews.com

**ADVANCED
HEALTHCARE
MATERIALS**

www.advhealthmat.de
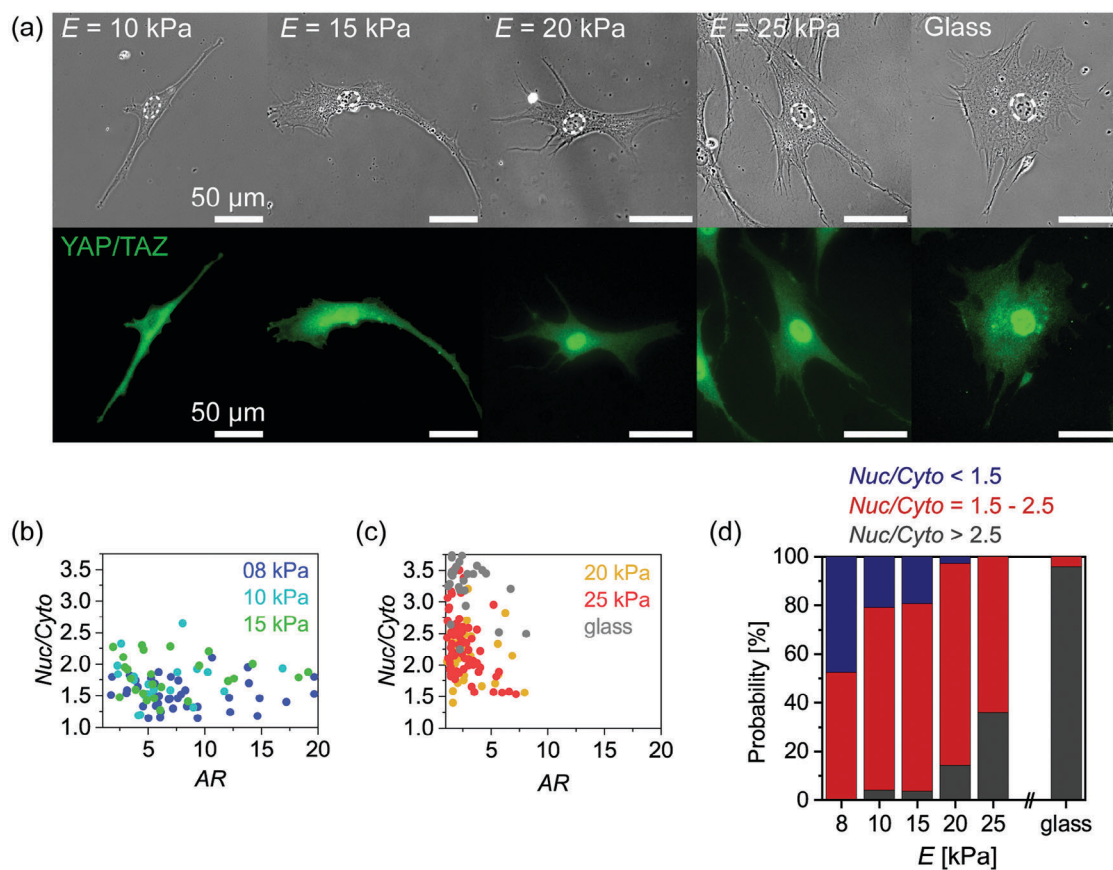
Figure 6. Nuclear translocation of YAP/TAZ is turned on at $E* > 20$ kPa. a) Phase contrast and immunofluorescence images of hMSCs stained with anti-YAP/TAZ antibody. b,c) Ratio of anti-YAP/TAZ signals in the nucleus (Nuc) to that in the cytoplasm (Cyto), Nuc/Cyto, plotted against aspect ratio AR, which can be categorized into two groups. Each dataset consists of data from $N \geq 27$ cells. d) Fractions of hMSCs with Nuc/Cyto < 1.5 (blue), Nuc/Cyto = 1.5–2.5 (red), and Nuc/Cyto > 2.5 (grey), indicating a sharp increase in the explicit nuclear localization at $E* \geq 20$ kPa.

establish their shape for 4 days. After confirming that the morphology of cells remained unchanged for 2 h, the substrate stiffness was switched at $t = 0$ h from $E = 25$ to 15 kPa, and changes in cell shape and traction forces over time were monitored (**Figure** 7a). It is important to note that the elasticity levels before and after the switching were only 5 kPa above or below $E* = 20$ kPa. Figure 7b shows the plot of the total strain energy U recorded over time for one representative cell. As shown in the figure, the elasticity was switched from stiff (red) to soft (blue), and the strain energy immediately decreased from 2.6 to 1.3 pJ. The strain energy then remained constant for the observed time period. In Figure 7c, U is plotted against A_{proj} from five different hMSCs (the average values and standard deviation of U are shown in Figure S16, Supporting Information). Each cell is indicated by color, and the open and solid symbols coincide with cells on stiff and soft gels, which means before and after the elasticity jump, respectively. Although A_{proj} showed a large scatter at both 25 and 15 kPa (see Figure 2c,e), the strain energy U exhibited a positive correlation with A_{proj} for both stiff and soft gels as shown under static conditions (Figure S15, Supporting Information), indicating that the correlation between U and A_{proj} was not violated even when the traction force instantaneously dropped within 10 min.

2.8. Turning YAP/TAZ Signaling On/Off by Elasticity Jump across $E*$

To gain kinetic insights into how mechanical stimulation is transduced to the cell nucleus, we monitored the dynamic changes in YAP/TAZ distribution over time. To compare the results with the change in traction force data (Figure 7), we first seeded cells on a stiff substrate ($E = 25$ kPa). We incubated cells for 4 days to give the cells enough time for adapting to the substrate stiffness ($E = 25$ kPa). After confirming that the morphology of cells remained unchanged for 2 h, the substrate stiffness was switched at $t = 0$ h from $E = 25$ to 15 kPa. **Figure 8a** shows the changes in anti-YAP/TAZ signals as a function of time. Once hMSCs established stable adhesion on the stiff substrate ($E = 25$ kPa), we observed a clear nuclear localization of YAP/TAZ, exemplified by the image at $t \leq 0$ h. At $t = 0$ h, the substrate was softened to $E = 15$ kPa. At $t = 3$ h, uniform YAP/TAZ distribution was already observed in the cytoplasm, and this was sustained as far as the Young's modulus E was set at 15 kPa. The substrate was then stiffened to $E = 25$ kPa by exchanging the medium three times between $t = 24$ and 27 h (Figure S3, Supporting Information). Notably, the recovery of nuclear YAP/TAZ signals to the initial level was only achieved at $t = 33$ h, which was 6 h after the completion of medium exchange.

**ADVANCED
SCIENCE NEWS**

www.advancedsciencenews.com

**ADVANCED
HEALTHCARE
MATERIALS**

www.advhealthmat.de
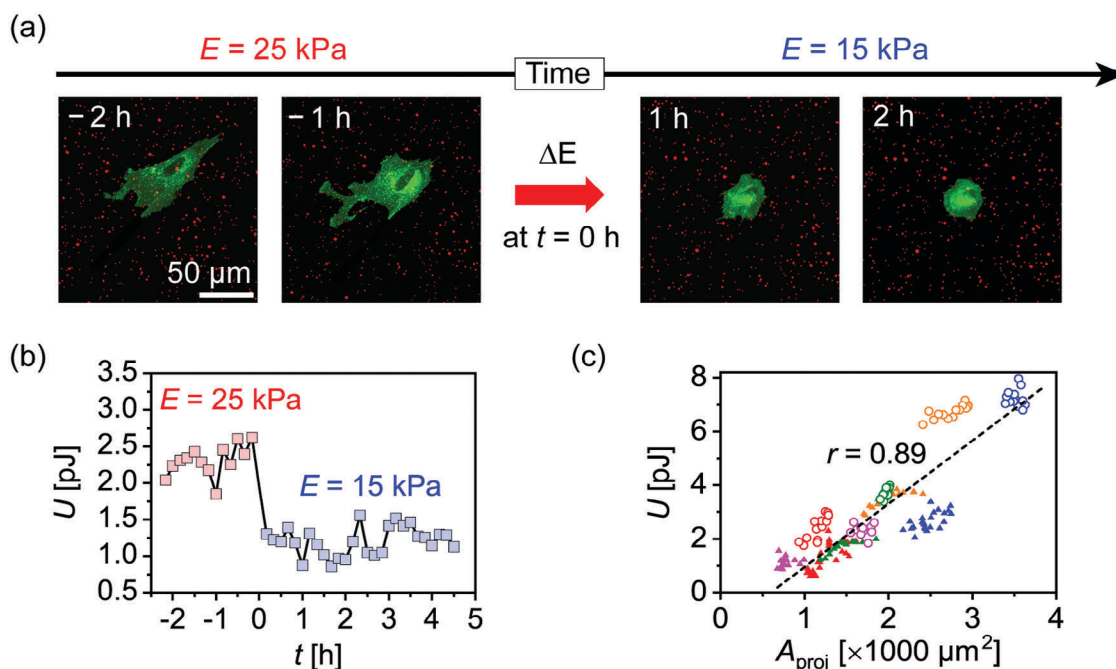
Figure 7. Changes in traction force upon elasticity jump across $E*$. a) Response of a cell to an abrupt decrease in the Young's modulus across $E* \approx$ 20 kPa. hMSCs were seeded on hydrogel substrates with $E = 25$ kPa for 4 days. The cell membrane was labeled with CellBrite (green). After confirming that the cell did not change the shape (after 2 h), the elasticity was switched to $E = 15$ kPa. Timelapse images were further collected for another 4 h with a time interval of $\Delta t = 10$ min. Red dots are fluorescently labeled nanoparticles used for the traction force analysis. b) The total strain energy U plotted versus time calculated from panel (a). The data of other cells are presented in Figure S16 (Supporting Information). Note that U decreased instantaneously upon softening. c) U–A_{proj} maps for 5× hMSCs. Each cell is indicated by color, and the open and solid symbols coincide with cells before and after the elasticity jump, respectively. The U–A_{proj} maps showed a clear positive correlation ($r = 0.89$).

Once the translocation was established, nuclear localization was sustained until the end of observation ($t = 123$ h).

To follow the dynamic modulation of YAP/TAZ signaling more quantitatively, we plotted the Nuc/Cyto ratio as a function of time for $N \geq 90$ cells at each time point (Figure 8b). Upon softening of the substrate by reducing $E = 25$ to 15 kPa, the median level of Nuc/Cyto exhibited a significant decrease from 3.0 to 2.3 at as soon as 3 h ($p < 0.001$), and this level remained unchanged over 24 h. The data obtained from another series of experiments performed at a higher time resolution ($\Delta t = 10$ min) showed that the fraction of cells with explicit nuclear YAP/TAZ expression $\chi_{nuclear}$ at $t = 50$ min is already 62% of the initial level (Figure S17, Supporting Information). As the decrease in Young's modulus was complete within 10 min, the monotonic decrease in $\chi_{nuclear}$ between $t = 10$ and 50 min indicated that it takes 40 min for hMSCs to turn off YAP/TAZ signaling by changing the substrate stiffness from 25 to 15 kPa. In contrast, upon the removal of free Ad-COONa in the medium, the Nuc/Cyto signal showed a significant increase ($p < 0.05$) from $t = 24$, 30, to 33 h. However, the recovery of the Nuc/Cyto signal was clearly slower than the decrease. In fact, the Nuc/Cyto level recovered the initial level only at $t = 33$ h, which is 9 h after the start of the medium exchange. Even if one takes the time required for the stiffening of the βCD–Ad gel by the medium exchange (Figure S3, Supporting Information) into account,[15c] it takes hMSCs 6 h to recover the YAP/TAZ signal. These data indicate that the kinetics of deactivation and reactivation of the YAP/TAZ signaling are distinctly different. The typical time required to deactivate the YAP/TAZ signaling (40 min) time

is almost an order of magnitude shorter than that required to reactivate YAP/TAZ (6 h).

As the YAP/TAZ signaling is mechanically regulated by the traction force generated by acto-myosin complex, we monitored the change in the morphological pattern representing the axial stretch (AR) and the spreading (A_{proj}) over time. As shown in Figure 8c, the AR–A_{proj} map at $t = 75$ h reproduced the one recorded at $t \leq 0$ h, which indicated that hMSCs reversibly switch not only the YAP/TAZ signaling but also the morphological patterns in response to the softening and stiffening of the substrate. The AR–A_{proj} maps at $t \leq 0$ h and $t \geq 75$ h are almost identical to the one recorded under the static substrate stiffness (Figure 2e), showing no sign of hysteresis. Because the AR–A_{proj} map recorded at $t = 3$ h reproduced the one taken at the static condition (Figure 2c), the AR–A_{proj} maps were also collected at a higher time resolution ($\Delta t = 10$ min) to follow the kinetics. As shown in Figure S17 (Supporting Information), the morphological pattern of the hMSC became unchanged already at $t = 50$ min. This indicates that the morphological transition and deactivation of YAP/TAZ occur with almost no delay. In contrast, the morphological patterns (AR–A_{proj} maps) needed much longer time to recover after the substrate stiffening. As mentioned above, the AR–A_{proj} map became identical to the static one only after 75 h, which is 48 h after the stiffening is complete. Remarkably, this time point (75 h) is more than 40 h after the re-establishment of nuclear localization of YAP/TAZ ($t = 33$ h), suggesting that the morphological adaptation follows the YAP/TAZ signaling. To the best of our knowledge, this is the first experimental study demon-
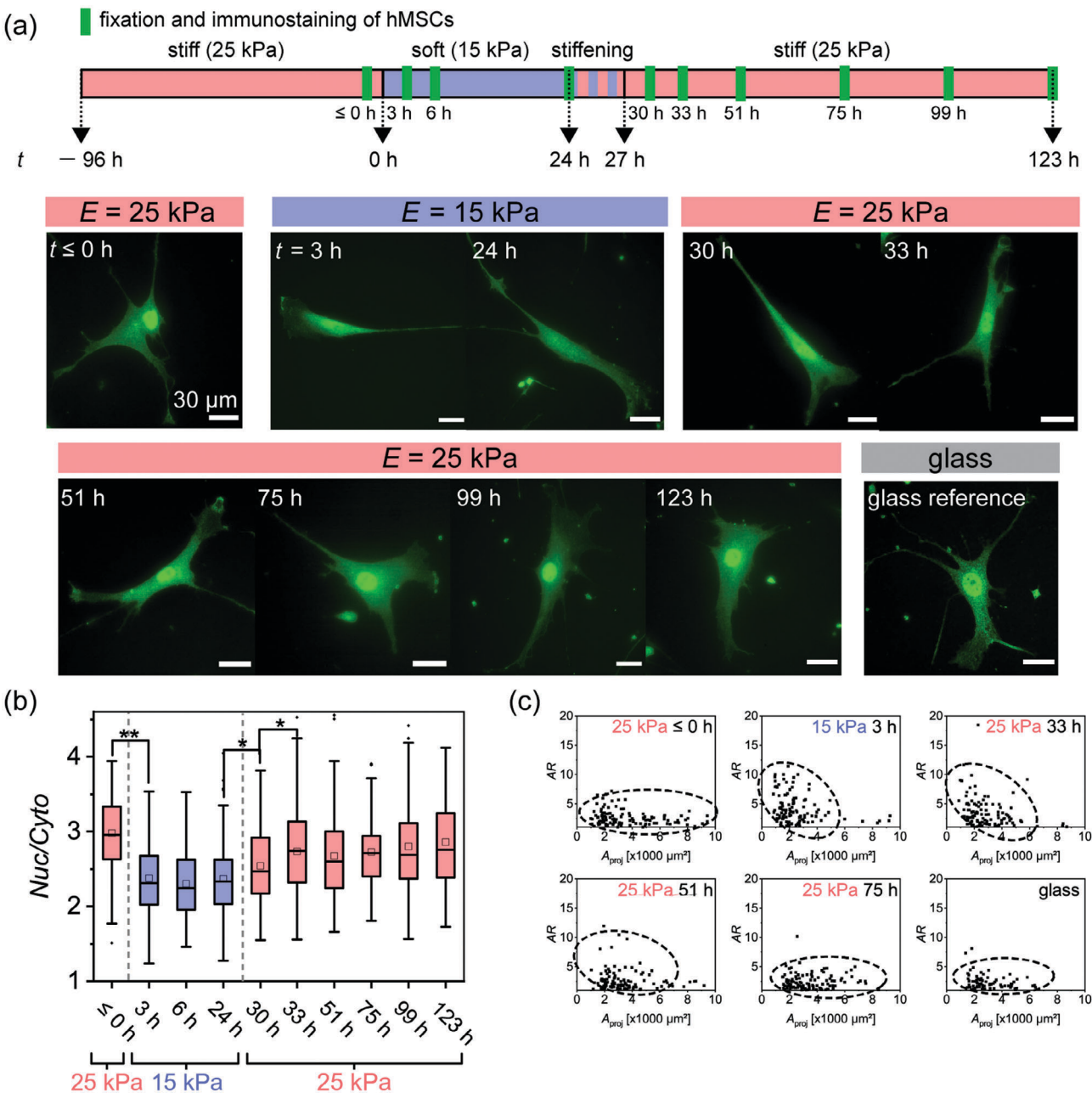
Figure 8. Turning YAP/TAZ signaling on/off by elasticity jump across E^*. a) Immunofluorescence images of hMSCs stained with anti-YAP/TAZ antibody at different time points. Hydrogel substrates were softened from 25 to 15 kPa at $t = 0$ h by exchange to medium containing 1.1 mM Ad-COONa. At $t = 24$ h the substrates were stiffened from 15 to 25 kPa by exchanging the medium every half an hour over a period of 3 h. b) Nuc/Cyto plotted over time. Each data point has been plotted based on $N \geq 90$ cells from two different samples per condition. The double asterisk indicates a significant difference with p-value < 0.001 and the single asterisk a significant difference with p-value < 0.05 by Student's t–test. c) Representative morphological patterns, AR versus A_{proj}, for the comparison with those collected under static conditions (Figure 2).

strating the differential on/off kinetics of YAP/TAZ signaling and the associated morphological adaptation of hMSCs in response to the reversible switching of the mechanical environment.[29a]

Proliferation and differentiation are the important fate decisions for stem cells. Once stem cells lose the control over their proliferation, this could cause many diseases like cancer. In contrast to terminally differentiated cells, hMSCs mostly remain in a dormant state and can rapidly respond to extrinsic stimuli for activation.[31] Proliferation, a crucial function of hMSCs in maintaining tissue homeostasis in vivo, is regulated by intrinsic cues like Wnt/β-catenin signaling, as well as by extrinsic stresses, such as oxidative stress.[32] Estrada et al. reported that culturing hMSCs under low oxygen conditions activates glycolysis, improving proliferation and genetic stability.[33] However, despite several studies suggesting the influence of mechanical stimuli such as shear stress or axial stretch on the lineage specific

2302607 (11 of 17)

**ADVANCED
SCIENCE NEWS**

www.advancedsciencenews.com

**ADVANCED
HEALTHCARE
MATERIALS**

www.advhealthmat.de
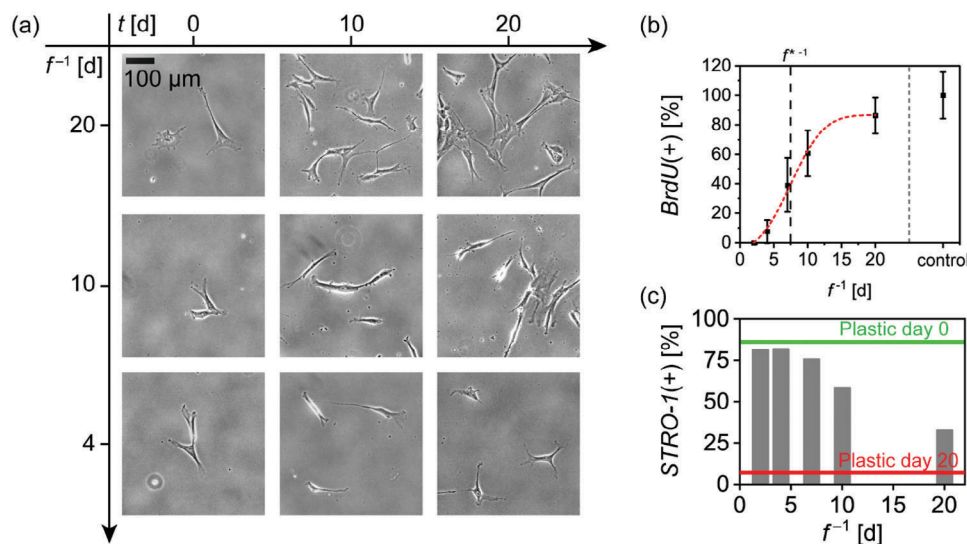
Figure 9. Frequent mechanical stimuli across E^* suppress hMSC proliferation. a) Effects of periodic mechanical stress on cell morphology and density. The substrate elasticity was altered to values between 25 and 8 kPa. Phase contrast images are shown for snapshots with different time t and periodicity f^{-1}. b) Fraction of cells showing positive immunoreactivity to BrdU (BrdU(+)) versus periodicity f^{-1} after 20 days. Each data corresponds to the mean and standard error calculated from >50 randomly selected regions of interest (0.4 mm² each). Fitting with the error function (black line) yielded the critical periodicity $f^{*-1} = 7.5$ days. c) Fraction of STRO-1(+) versus periodicity f^{-1} after 20 days. Compared to the control level on plastic dishes showing a significant decrease in p from 85% (green line) to 7% (red line) in 20 days, hMSCs on hydrogel substrates showed higher immunoreactivity. Note that a frequent switching of substrate stiffness at shorter periodicities of $f^{-1} \leq 4$ days suppressed the hMSC proliferation (<10% of the control), while the STRO-1(+) level (80%) was maintained close to the initial level (85%).

differentiation of hMSCs,[34] little is known about the effects of mechanical stimuli on hMSC proliferation.[35] Aragona et al. showed that the proliferation capacity of multicellular sheets is regulated via mechanical stresses, such as stretching, location at edges/curvatures contouring an epithelial sheet, or stiffness of the surrounding extracellular matrix.[36] Such biomechanical cues from the microenvironment influence the activity of signaling pathways, including Wnt, Notch, and YAP/TAZ pathways, in tumorigenesis and intestinal regeneration.[36,37] Yet, the influence of the significance and frequency of the mechanical stress on the proliferation capacity of hMSCs is not known.

Our supramolecular hydrogel substrates are optimally designed to investigate the impact of dynamic mechanical stress with defined magnitude (ΔE) and defined frequency (f), because the Young's moduli of substrates can be switched across E^* in a reversible manner on-demand. Thus, we monitored hMSC proliferation by varying the frequency of mechanical stimuli, f. The left, middle, and right columns of **Figure 9a** show snapshots of hMSCs taken at $f^{-1} = 4$, 10 and 20 days, where "$f^{-1} = x$ days" means that substrate stiffness was changed between 25 and 8 kPa every x days. Notably, the number density of cells determined from randomly selected more than 20 fields of view on $t = 20$ days, suggested that the proliferation was suppressed when cells are more frequently stressed (Figure S18, Supporting Information). Therefore, we performed the BrdU assay and determined the fraction of BrdU positive cells (BrdU(+)) as a function of f^{-1} (Figure 9b). Compared with the control hMSCs with substrates having a constant value of $E = 25$ kPa ($f^{-1} = 20$ days), more frequent changes in substrate stiffness resulted in a monotonic decrease in BrdU(+). Fitting of the data with an error function (red line) indicated that BrdU(+) became less than 50% of the control at $f^{*-1} = 7.5$ days. Notably, a frequent switching of substrate stiff-

ness at shorter periodicities of $f^{-1} \leq 4$ days resulted in BrdU(+) level less than that of 10% of the control, demonstrating that the frequency f of mechanical stress across E^* plays dominant roles in the suppression of hMSC proliferation.

However, as the value of BrdU(+) cannot discriminate differentiated cells from non-differentiated cells, we evaluated the fraction of STRO-1 immunoreactive cells, a marker used to sort hMSCs with multiple lineage potentials.[14c,38] Figure 9c shows the percentage of STRO-1 positive cells (STRO-1(+)) at $t = 20$ days. For comparison, the STRO-1(+) levels on plastic dishes at $t = 0$ (green) and 20 days (red) are presented, showing a significant decrease in STRO-1(+) from 85% to 7% in 20 days, as reported previously.[14c,38b] In contrast, the STRO-1(+) fraction of hMSCs grown on host–guest gels with a constant stiffness for 20 days (30% for both 25 and 8 kPa) was distinctly higher than those seeded on plastic dishes (7%). More remarkably, when the substrate stiffness was switched more frequently than every 4 days ($f^{-1} \leq 4$ days), the STRO-1(+) level reached 80%, which is comparable to the initial level (85%). These data demonstrated that more than 90% of hMSCs stopped the proliferation under a frequent switching of substrate stiffness ($f^{-1} \leq 4$ days) with no loss of multipotency.

3. Discussion

3.1. Mechanosensing of hMSCs to Static Substrate Stiffness

When the static stiffness of our polyacrylamide-based βCD–Ad gel (3,3) was varied from $E = 8$, 10, 15, 20, to 25 kPa by changing [Ad-COONa], the morphological patterns of hMSCs, represented by AR–A_{proj} maps, showed a clear change (Figure 2). On soft hydrogels ($E = 8$ and 10 kPa), the spreading of hMSCs (A_{proj}) was

not pronounced ($<2500\ \mu m^2$) but the elongation (AR) showed a large scatter, suggesting that the cells are free to take any shape but the total area that they can spread is limited. In contrast, on stiff hydrogels ($E = 20$ and 25 kPa), hMSCs took a similar shape (AR < 10), while the spreading area (A_{proj}) scatters over a wide range, suggesting that the cells have an optimal shape independent from how much they spread. The observed tendency is in line with the previous report on RGD peptide-functionalized hyaluronic acid gels with different degrees of covalent crosslinks ($E = 1$, 5, and 20 kPa).[29b] Interestingly, the further increase in the gel stiffness, even up to the non-physiological level (400 kPa), did not change the morphological patterns (Figure S5, Supporting Information), indicating that the morphology of hMSCs is no longer sensitive to the stiffness beyond 20 kPa.

As reported by Dupont et al. by using micropatterns of ECM proteins on glass/plastic substrates and soft (0.7 kPa) and stiff (40 kPa) gels, the spreading of cells play key roles in the YAP/TAZ signals.[11c] As both the size (A_{proj}) and shape (AR) of cells are defined by the focal adhesion and actin cytoskeleton, we determined the total area of focal adhesions and calculated the nematic order parameter of actin cytoskeletons from the immunohistochemical images (Figure 3).[18,22c,27] The focal adhesion area showed a monotonic increase with increasing E. The hMSCs on the softest gel (8 kPa) showed a significantly smaller focal adhesion area compared to those on stiff gels (20 and 25 kPa), and the order parameter of actin stress fibers, weighted by the length and the thickness, showed a statistically significant difference between soft and stiff substrates. Note that the differences were screened due to the large scatters in size (A_{proj}) at lower E and those in the elongation (AR) at higher E (Figure 2). The treatment of cells with the inhibitors for non-muscle myosin II and Rho resulted in a significant decrease of cells with explicit nuclear YAP/TAZ signals (Figure S19, Supporting Information), confirming that the cell traction forces guides the YAP/TAZ localization. In fact, the traction force microscopy analysis (Figure 4) indicated that net contractile moment μ plotted versus the degree of axial elongation (AR) exhibited a distinct transition between soft gels (8 and 10 kPa) and stiff gels (25 kPa). The 25–75 percentile range of μ increased from 1–3 nJ (soft gels) to 4–9 nJ (stiff gels), because μ is the contractile moment parallel the principal axis of elongation.

The changes in the focal adhesion area and the directional order of actin stress fibers (Figure 3) between soft and stiff gels suggest the modulation of the cell adhesion force. Using our self-built setup,[27,28b] we evaluated mechanical strength of the adhesion of hMSCs to hydrogel substrates (Figure 5). It should be noted that the mechanical response of cells is purely elastic, because the cells interact with the ultrasonic shockwave for only ≈80 ns. This methods enabled to evaluate the mechanical strength of cell adhesion with statistically reliable sample sizes for various cells, such as malaria-infected human erythrocytes, donor-derived human hematopoietic and progenitor cells, and human induced pluripotent cells.[28,39] The detached cells are able to adhere to a new location, because this is a non-invasive, probe free technique, which is distinct from other techniques, such as pulling a magnetic particle attached to a cell or pulling/peeling off a cell from the adhesive substrate using an AFM tip.[40] Notably, as a previous AFM study demonstrated, higher loading rates result in stronger interactions between ligand–receptor interactions.[41] By converting the loading rates in the order of 10^6 s^{-1} to a stress/pressure,[27,42] this yields the comparable values to our experimentally determined P^* values that are in the order of MPa. The critical pressure P^* showed a significant increase from $P^* = 4.2$ MPa ($E = 20$ kPa) and $P^* = 5.0$ MPa ($E = 25$ kPa) with $p < 0.001$. In contrast, the width of transition, represented by the FWHM of $\delta\chi/\delta P$, exhibited a continuous decrease with increasing E, which can be attributed to a more pronounced and widely distributed elongation of cells (AR), as shown in Figure 2.

As all the above-mentioned data indicated $E^* \approx 20$ kPa as the critical substrate stiffness beyond which hMSCs switch the mechanical response to the substrate's Young's modulus. Previously, Dupont et al. observed a pronounced nuclear localization of YAP/TAZ in hMSCs on covalently crosslinked polyacrylamide gels with Young's modulus $E = 40$ kPa but not on gels with $E = 0.7$ kPa.[11c] By comparing the data on gels and those on micropatterns of fibronectin on glass slides, they attributed the nuclear localization of YAP/TAZ to the tension induced by actin cytoskeletons. However, the critical threshold stiffness for the mechanosensing of hMSCs could not be determined, because the intermediate stiffness levels have not been examined. Caliari et al. reported Nuc/Cyto values in hMSCs seeded on chemically crosslinked hyaluronic acid gels (1, 5, and 20 kPa) functionalized with RGD peptides,[29b] but the difference in Nuc/Cyto values between 5 and 20 kPa was not statistically significant. Kuroda et al. seeded mouse MSCs on covalently crosslinked, collagen-coated polyacrylamide gels (1.5, 3.2, and 8.7 kPa) and reported the critical role of focal adhesions (vinculin).[9] Although they observed a monotonic increase in Nuc/Cyto rations with increasing substrate stiffness, no critical stiffness was determined, probably because the stiffness range they examined was lower than E^*. In this study, we found that the fraction of cells showing explicit nuclear localization (Nuc/Cyto > 2.5) was <4% on soft gels ($E = 8$–15 kPa), but this showed a marked increase to 14.3% (20 kPa) and 36.1% (25 kPa) with increasing substrate stiffness (Figure 6), confirming that the YAP/TAZ signaling pathway is turned on. Moreover, the cells on soft and stiff gels can be clearly distinguished by the combination of Nuc/Cyto and AR (Figure 6). Together with the positive correlation between Nuc/Cyto and A_{proj} (Figure S15, Supporting Information), we concluded that the traction force in the direction of axial stretch directs the nuclear localization of YAP/TAZ. Notably, the distinctly different response of hMSCs to a subtle difference in the substrate stiffness, such as $E = 15$ and 25 kPa, suggests that hMSCs sensitively detect a small change in their mechanical environments and adapt their shape, traction force, and intracellular signaling. Although this study explicitly dealt with isolated hMSCs, it is plausible that not only the cell–matrix interactions but also the cell–cell interactions also modulate the mecahnosensing of hMSCs. To mimic the cell–matrix and cell–cell interactions, Cosgrove et al. functionalized the chemically crosslinked hyaluronic acid gels with ligand motifs for integrin and N-cadherin, and showed that the N-cadherin–mediated adhesion reduces the traction force, which increased the onset of YAP/TAZ signaling to a higher E levels.[43]

3.2. Mechanosensing of hMSCs to Dynamic Substrate Stiffness

To date, several materials have been designed to investigate the response of hMSCs to dynamic substrate stiffness. For example,

Guvendiren and Burdick fabricated methacrylated hydronic acid gels crosslinked by thiols and observed how hMSCs respond to the stiffening of gels from $E = 3$ to 30 kPa.[14a] They reported the stiffening facilitated the spreading and increase in the traction stress in short term and the differentiation bias toward the osteogenic lineage. Killaars et al. showed that the softening of polyethyleneglycol (PEG)-based hydrogels by the fragmentation of allyl sulfide crosslinkers from $E = 33$ to 6 kPa leads to the delocalization of YAP and condensation of chromatin occurred in the first few hours after softening.[14b] However, both systems allow only one-directional change in substrate elasticity, either from "soft-to-stiff" or "stiff-to-soft," but these materials cannot switch the stiffness of the same substrate in a reversible manner. Frank et al. utilized pH responsive hydrogels based on ABA tri-block copolymers, whose stiffness could be reversibly switched between 2 and 40 kPa by changing the pH between 6.6 and 7.5.[14c]

As the supramolecular βCD–Ad gels can reversibly switch the stiffness on-demand, they offer a unique possibility to monitor how hMSCs detect and respond to the dynamic softening and stiffening of the substrates with a finer step in situ. In contrast to the previous studies changing the substrate elasticity by a large step, $\Delta E \approx 30$–40 kPa, we utilized a subtle change in the stiffness across $E^* \approx 20$ kPa as the mechanical cue. As shown in Figure 7, the softening of the gel from 25 to 15 kPa is immediately followed by the decrease in the total strain energy U by a factor of two. It is notable that the decrease in the strain energy occurred almost instantaneously. Moreover, the strain energy integrated over each cell shows a positive correlation with A_{proj}, which seems reasonable that the total strain energy scales with the cell–substrate contact. Unfortunately, it is not practically possible to extend the duration of timelapse confocal imaging in response to the substrate stiffness because the recovery of A_{proj} needs several hours.

The dynamic response of YAP/TAZ signaling was more quantitatively monitored by the immunofluorescence determination of Nuc/Cyto ratios during the stiffening and softening of βCD–Ad gels (Figure 8). The experiments at higher time resolution ($\Delta t = 10$ min) unraveled that the YAP/TAZ de-localization is complete already at $t = 50$ min. As the softening is complete in 10 min, this finding indicates that the silencing of YAP/TAZ takes 40 min after switching the stiffness from 25 to 15 kPa. This seems to be in good agreement with the previous study, reporting that the YAP/TAZ is delocalized after 1 h of the substrate softening from 33 to 6 kPa.[14b] Our data demonstrated that only a $\Delta E = 10$ kPa step across E^* is sufficient to deactivate YAP/TAZ signaling. In contrast, the reactivation of YAP/TAZ signaling by substrate stiffening took much longer. By taking the time for the substrate stiffening by the medium exchange (3 h), a clear recovery was confirmed only after 6 h, indicating that the characteristic time needed for turn on YAP/TAZ signaling is by one order of magnitude longer. These data suggest that the supramolecular hydrogels can be used to further investigate the mechanical memory of hMSCs.[14b,44] It is well established that the in vitro expansion of hMSCs on stiff substrates, such as polystyrene-based culture flask, causes the decrease in the regenerative functions of transplanted hMSCs.[14b,45] Using allyl sulfide-crosslinked PEG substrates, Yang et al. reported that the YAP/TAZ signal showed a clear hysteresis depending on how long they were exposed to stiff substrates.[44] They showed that the fraction of cells show-ing nuclear YAP localization did not converge to that of hMSCs always on 2 kPa gels even after photo-induced softening, once they are exposed for 7 days or longer to plastic or $E = 10$ kPa gels. Using hyaluronic acid gels functionalized with integrin and N-cadherin ligands, Zhang et al. reported that such a mechanical memory can be erased by transplanting the cells from stiff plastic substrates to the gels with N-cadherin ligands.[46] In this study, we focused on the isolated hMSCs with no cell–cell contact and found that the Nuc/Cyto level of hMSCs after softening from 25 to 15 kPa was comparable to the hMSCs cultured always on 8 kPa gel, showing no sign of hysteresis.

Taking the unique advantage of βCD–Ad gels that can reversibly switch the substrate stiffness on-demand, we investigated if the frequency of mechanical stimuli f would affect the proliferation capacity and multipotency of hMSCs by periodically switching the stiffness across E^* over 20 days (Figure 9). Prior to the experiments, we examined if βCD–Ad gels are able to reversibly switch the stiffness over long time. As shown in Figure S20 (Supporting Information), we confirmed that the substrate stiffness can be reversibly switched with no sign of hysteresis by measuring the Young's modulus under the exchange of medium with and without 5 mM Ad-COONa at the highest frequency ($f^{-1} = 2$ days) over 20 days. This result guarantees the chemical and mechanical stability of βCD–Ad gels as the dynamic stem cell culture materials over weeks. Moreover, as reported previously, hMSCs produce new ECM proteins, such as fibronectin,[47] and they might affect the stiffness of βCD–Ad gels. To exclude the possibility, we performed the immunofluorescence staining of fibronectin and AFM indentation at $t = 4$, 14, and 20 days. Although the precise determination of produced fibronectin was technically not possible due to the fact that the surface of βCD–Ad gel was functionalized with fibronectin (Figure S2, Supporting Information), we detected the newly produced fibronectin as an increase in the fluorescence signals. However, as shown in Figure S21 (Supporting Information), we observed no change in the E values after the culture of hMSCs over 20 days. This could partly be attributed to the fact that we seeded hMSCs sparsely on βCD–Ad gels and studied the single cell behaviors.

When we applied the mechanical stimuli with different periodicities (f^{-1}), we found that a frequent switching of substrate stiffness at shorter periodicities of $f^{-1} \leq 4$ days resulted in BrdU(+) level less than that of 10% of the control, while the STRO-1(+) level (80%) was maintained close to the initial level (85%). These results demonstrated that frequent mechanical stimulation of hMSCs across E^* significantly suppressed proliferation without reducing multipotency. The critical periodicity to suppress hMSC proliferation, $f^{*-1} \approx 7.5$ days, is consistent with previous data on pH-responsive hydrogels ($f^{*-1} \approx 7$ days),[14c] despite the fact that the materials, chemical stimuli, and the extent of change in stiffness ($\Delta E \approx 40$ kPa) are all different in this study. This suggests that the frequency f of mechanical stress across E^* plays more dominant roles in regulating the proliferation and multipotency maintenance than the magnitude of stiffness change ΔE. Further studies on the influence of stress frequency on the gene expression patterns via transcription factor and/or epigenetics would unravel the potentials of this material to overcome the major problems of plastic culture dishes, such as overgrowth and loss of multipotency of hMSC.

**ADVANCED
SCIENCE NEWS**

www.advancedsciencenews.com

**ADVANCED
HEALTHCARE
MATERIALS**

www.advhealthmat.de

4. Conclusions

Using supramolecular hydrogels with reversible host–guest (βCD-Ad) crosslinks, we have demonstrated the mechanical regulation of hMSCs by applying static and dynamic mechanical stimuli on-demand. Simply by adding or removing non-cytotoxic free guest (Ad-COONa) molecules to the culture medium, the stiffness (Young's modulus E) of hydrogel substrates can be switched reversibly to the desired E level. Once the surface functionalization was optimized and the hydrogel substrates were calibrated, we observed distinctly different morphological patterns at $E^* \geq 20$ kPa. Traction force field analysis indicated that the net contractile moment μ on stiff substrates ($E = 25$ kPa) was five times larger than that on soft substrates ($E = 8$ kPa). Moreover, with aid of a non-invasive assay utilizing a shock wave induced by a ps laser pulse, we confirmed that the cell adhesion strength distinctly increased between $E = 20$ and 25 kPa. The transition of the mechanical interactions between hMSCs and hydrogel substrates triggered the translocation of the transcription factors YAP/TAZ to cell nuclei. We monitored the dynamic response of hMSCs to the abrupt change in substrate stiffness across E^* using traction force analysis, indicating an instantaneous drop in the strain energy upon softening. Further, we tracked the translocation of YAP/TAZ and found the distinctly different kinetics of the YAP/TAZ deactivation and reactivation. Notably, the original morphology was recovered 40 h only after YAP/TAZ reached the saturation level, indicating that morphological adaptation of hMSCs follows the mechanosensing.

To investigate the potential biomedical applications of our supramolecular hydrogels, we assessed whether periodic mechanical stimulation could affect the self-renewal capacity of hMSCs. Our findings revealed that the surface density of hMSCs subjected to changes in substrate stiffness every 2 days was approximately five times lower than that of cells maintained on substrates with constant stiffness. This indicates that frequent mechanical stress significantly inhibits hMSC proliferation. Furthermore, immunofluorescence staining of STRO-1, a surface marker for multiple lineage potentials, demonstrated that frequent stress, such as switching substrate stiffness every four or less, suppress the proliferation and maintain the multipotency. It is notable that the frequency of mechanical stress seems to play more dominant roles than the magnitude of stiffness change in regulating the functions of hMSCs.

Thus, supramolecular hydrogel substrates with switchable stiffness *on demand* represent a promising alternative to commonly utilized plastic culture dishes and flasks and chemically crosslinked hydrogels for the stable culture of primary hMSCs from donors.

5. Experimental Section

Chemicals: Ammonium-peroxodisulfate (APS) and tetramethylethylenediamine (TEMED) were purchased from Bio-Rad (Hercules, CA, USA). Vinyl trimethoxysilane 98 % was obtained from VWR (Wayne, PA, USA). Polydimethylsiloxane (PDMS, Sylgard 184) was purchased from Dow Corning (Midland, MI, USA). Mesenchymal stem cell growth medium (MSCGM) was purchased from Lonza (Basel, Switzerland). Texas Red-X Phalloidin, STRO-1 antibody, vinculin monoclonal antibody (7F9), Alexa Fluor 488, Goat anti-mouse IgG, IgM (H+L) secondary anti-

body, Alexa Fluor 488, and STRO-1 monoclonal antibody (STRO-1) were obtained from Thermo Fisher Scientific (Waltham, MA, USA). Anti-YAP antibody was purchased from Santa Cruz Biotechnology (Dallas, TX, USA). CellBrite green was purchased from Biotium (Fremont, CA, USA). Bovine serum albumin (BSA) and Triton X-100 were purchased from Carl Roth (Karlsruhe, Germany). (−)-Blebbistatin was purchased from Sigma-Aldrich (St. Louis, MO, USA) and Rho inhibitor C3 was obtained from Cytoskeleton, Inc. (Denver, CO, USA). Unless stated otherwise, all other chemicals were purchased from Sigma-Aldrich (St. Louis, MO, USA) and used without further purification.

Supramolecular Hydrogel (βCD–Ad Gel) Substrate: Prior to the βCD–Ad gel deposition, round glass slides with diameters of 20 and 25 mm were cleaned using the modified RCA method.[48] The glass slides were coated with vinyl trimethoxysilane to immobilize the βCD–Ad gel covalently. The βCD–Ad gel was prepared as described previously.[15b] Briefly, 6-acrylamido–βCD βCD-AAm (71.3 mg, 3 mol%) and adamantane-acrylamide Ad-AAm (12.3 mg, 3 mol%)[49] were dissolved in distilled water (1 mL) by stirring at 90 °C for 3 h. After cooling to 20 °C, acrylamide AAm (133.6 mg, 94 mol%) and APS (4.6 mg, 1 mol%) were added to the βCD–Ad solution. Polymerization was initiated by adding TEMED (0.3% v/v) to the monomer solution, and a 25 µL portion of the monomer-TEMED solution was deposited on the vinyl-silanized glass. Of note, N,N'-acrylamide was added up to 1.35% w/v to prepare substrates with higher Young's modulus. To prepare flat films, a glass slide was placed on top for 15 min. After removing the plain glass slide, the sample was soaked in a mixed solvent of water/DMSO = 1/1 v/v for 1 day and in distilled water for 2 days to remove monomers and TEMED. The glass coated with βCD–Ad gel was glued to the bottom of a petri dish using PDMS. Fibronectin was covalently bound to the substrate surface using the Sulfo-SANPAH photocrosslinker.[15b,50] The elasticity (Young's modulus) of the βCD–Ad gel was measured using an atomic force microscope (NanoWizard, JPK Instruments, Berlin, Germany) and a colloidal probe cantilever (CP-qp-CONT-BSG-B, NanoAndMore, Wetzlar, Germany) with a diameter of 10 µm and a spring constant of $k = 0.08$–0.15 N m^{-1}.[15c]

Cell Culture: The hMSCs were isolated and cultured as previously described.[51] Bone marrow samples were obtained from healthy donors after obtaining written consent. This was done following guidelines approved by the Ethic Committee on the Use of Human Subjects at Heidelberg University. The mononuclear cell fraction was isolated via density gradient centrifugation and seeded in plastic culture flasks at a density of 100 000 MNCs cm^{-2} in MSCGM (Lonza, Basel, Switzerland). hMSCs were cultured in MSCGM, with the medium being renewed every 2 days. The cells were expanded by splitting the colonies after 10–14 days of culture. For this study, hMSCs from early passages (<8) were used. To monitor the response of single cells, hMSCs were seeded at a density of 500 cells on stiff gels ($E = 25$ kPa). The cells were incubated for 4 days to ensure that they can adapt to the substrate stiffness ($E = 25$ kPa). After confirming that the cell morphology remained unchanged over 2 h, the cells were subjected to the image acquisition and the dynamic stimuli. The substrate elasticity was then adjusted using [Ad-COONa]. The inhibitor experiments were performed by incubating hMSCs with 50 µм blebbistatin (myosin II blocker, Sigma-Aldrich; St. Louis, MO, USA) or 3 µg mL^{-1} C3 (Rho inihbitor, Cytoskeleton, Inc.; Denver, CO, USA) for 4 h.

Immunocytochemistry: Immunostaining was performed to visualize cell nuclei, actin filaments, the focal adhesion protein vinculin, and the transcriptional coactivators YAP/TAZ. To visualize the active, cytoskeleton-bound vinculin in cells, the cells were incubated with CSK buffer (0.5% w/v Triton X-100, 10 mм PIPES pH 6.8, 50 mм NaCl, 3 MgCl$_2$, and 300 mм sucrose) for 1.5 min at 4 °C, followed by immediate fixation with 4% w/v paraformaldehyde (PFA) in PBS for 15 min at room temperature. Otherwise, the cells were fixed using 4% PFA in PBS for 15 min at room temperature. After fixation, the cells were washed with PBS three times for 5 min and subsequently incubated for 5 min with 0.2% Triton X-100 for permeabilization. The cells were then blocked with 3% w/v BSA in PBS for 30 min at room temperature. The following primary antibodies were used: vinculin monoclonal antibody (7F9) conjugated with Alexa Fluor 488 (1:200), anti-YAP (1:100), anti-STRO-1 (1:200), and Texas Red Phalloidin (1:800). The cells were incubated with the primary antibodies in 3% BSA overnight at

4 °C (anti-vinculin and anti-YAP) or for 1 h at room temperature (anti-STRO-1 and Phalloidin). Samples were again washed and incubated with fluorescence tagged secondary antibodies (Alexa Fluor 488 Goat anti-mouse) for 1 h at room temperature. Finally, the nuclei were stained with DAPI (1:1000) for 10 min in PBS. The stained cells were stored at 4 °C in the dark.

Image Acquisition and Analysis: Images were acquired using a Nikon C2 Plus confocal microscope that was equipped either with a 60× water immersion objective or a 40× oil immersion objective, or with a Zeiss AxioObserver using a 40× oil objective. The analysis of cell morphology was performed using Fiji software.[52] The nematic order parameter of actin cytoskeletons $\langle S \rangle$ was calculated using a custom routine in MatLab (MathWorks, Natick, USA), as described previously.[18,22] The complete procedure is described in Figure S8 (Supporting Information). The size and distribution of focal adhesions (FA) were performed semi-automatically using maximum intensity projection and binarization by an automatic intensity threshold using the MaxEntropy method in Fiji software. All connected areas with the size of 1–20 µm^2 were classified as FA.

The localization of YAP/TAZ was assessed following previous reports.[29b,c,43] After segmentation, the fluorescence signals from the nucleus and the rest of the cytoplasm were separated from the whole cell, yielding the nuclear-to-cytoplasmic ratio (Nuc/Cyto) of YAP/TAZ, Nuc/Cyto (Figure S13, Supporting Information). The YAP/TAZ distribution was classified into three categories: Nuc/Cyto < 1.5, Nuc/Cyto = 1.5–2.5, and Nuc/Cyto > 2.5.

Traction Force Microscopy: The aqueous suspension of fluorescent beads (diameter: 0.2 µm, Thermo Fisher Scientific, Waltham, MA, USA) was spread onto the cleaned glass. After evaporation of water, the glass substrate was flipped upside-down and placed onto the monomer-TEMED solution undergoing polymerization. This process enabled the confinement of the beads on the surface of βCD–Ad gel. Traction force analysis was performed using MATLAB (MathWorks, Natick, MA, USA). As reported previously,[24,25] the movement of fluorescent beads was tracked using PIV. The stress was calculated from the extracted 2D vector field using the Boussinesq function.

Determination of Cell Adhesion Strength with Pressure Wave: The strength of cell adhesion was quantitatively assessed using this self-developed instrument that employed ultrasound pressure waves generated by a ps laser pulse.[27,28,39a] An infrared laser pulse ($\lambda = 1064$ nm, $\tau_L \approx 30$ ps) from Nd:YAG (EKSLPLA, Vilnius, Lithuania) was focused through a 10× objective into a cell incubation chamber mounted on an inverted microscope (Eclipse TE2000-U, Nikon Europe). The pressure was calibrated as a function of pulse energy and distance from the focus, using a piezoelectric pressure sensor (Müller Instruments, Oberursel, Germany). Before and after the exposure to the pressure wave, bright field microscopy images were captured in the form of a 5 × 5 tile. Cells that remained adherent after the pressure wave exposure were manually marked using Fiji software. The complete procedure is described in Figures S10 and S11 (Supporting Information).

Statistical Analysis: Statistical analysis of data was performed using Origin Pro 2019 (Origin Lab, Northampton, MA, USA). All box plots presented in this study present the median value as a solid line and the average value as a square. The boxes correspond to the 25–75 percentile ranges, and the whiskers to the 5–95 percentiles. Normal distribution of data was assumed. Student's *t*-test was performed for comparison between two groups. The *p* values < 0.05 were considered as significant difference.

Supporting Information

Supporting Information is available from the Wiley Online Library or from the author.

Acknowledgements

Conflict of Interest

The authors declare no conflict of interest.

Data Availability Statement

The data that support the findings of this study are available from the corresponding author upon reasonable request.

Keywords

[1] C. Bonnans, J. Chou, Z. Werb, *Nat. Rev. Mol. Cell Biol.* **2014**, *15*, 786.
[2] a) O. Chaudhuri, J. Cooper-White, P. A. Janmey, D. J. Mooney, V. B. Shenoy, *Nature* **2020**, *584*, 535; b) B. J. Dzamba, D. W. DeSimone, *Curr. Top. Dev. Biol.* **2018**, *130*, 245.
[3] a) R. J. Pelham, Y.-L. Wang, *Proc. Natl. Acad. Sci. USA* **1997**, *94*, 13661; b) A. Engler, L. Bacakova, C. Newman, A. Hategan, M. Griffin, D. Discher, *Biophys. J.* **2004**, *86*, 617.
[4] A. J. Engler, M. A. Griffin, S. Sen, C. G. Bonnemann, H. L Sweeney, D. E. Discher, *J. Cell Biol.* **2004**, *166*, 877.
[5] a) A. J. Engler, S. Sen, H. L Sweeney, D. E. Discher, *Cell* **2006**, *126*, 677; b) S. Rammensee, M. S. Kang, K. Georgiou, S. Kumar, D. V. Schaffer, *Stem Cells* **2017**, *35*, 497; c) K. Ye, X. Wang, L. Cao, S. Li, Z. Li, L. Yu, J. Ding, *Nano Lett.* **2015**, *15*, 4720.
[6] a) L. Przybyla, J. N. Lakins, V. M. Weaver, *Cell Stem Cell* **2016**, *19*, 462; b) J. M. Muncie, V. M. Weaver, *Curr. Top. Dev. Biol.* **2018**, *130*, 1.
[7] H. Kanazawa, Y. Fujimoto, T. Teratani, J. Iwasaki, N. Kasahara, K. Negishi, T. Tsuruyama, S. Uemoto, E. Kobayashi, *PLoS One* **2011**, *6*, e19195.
[8] a) C. E. Chan, D. J. Odde, *Science* **2008**, *322*, 1687; b) L. B. Case, C. M. Waterman, *Nat. Cell Biol.* **2015**, *17*, 955; c) A. Elosegui-Artola, R. Oria, Y. Chen, A. Kosmalska, C. Pérez-González, N. Castro, C. Zhu, X. Trepat, P. Roca-Cusachs, *Nat. Cell Biol.* **2016**, *18*, 540; d) K. A. Jansen, P. Atherton, C. Ballestrem, *Semin. Cell Dev. Biol.* **2017**, *71*, 75.
[9] M. Kuroda, H. Wada, Y. Kimura, K. Ueda, N. Kioka, *J. Cell Sci.* **2017**, *130*, 989.
[10] A. Pocaterra, P. Romani, S. Dupont, *J. Cell Sci.* **2020**, 133, jcs23042562.
[11] a) A. Totaro, T. Panciera, S. Piccolo, *Nat. Cell Biol.* **2018**, *20*, 888; b) S. Porazinski, H. Wang, Y. Asaoka, M. Behrndt, T. Miyamoto, H. Morita, S. Hata, T. Sasaki, S. F. G. Krens, Y. Osada, S. Asaka, A. Momoi, S. Linton, J. B. Miesfeld, B. A. Link, T. Senga, A. Castillo-Morales, A. O. Urrutia, N. Shimizu, H. Nagase, S. Matsuura, S. Bagby, H. Kondoh,

H. Nishina, C.-P. Heisenberg, M. Furutani-Seiki, *Nature* **2015**, *521*, 217; c) S. Dupont, L. Morsut, M. Aragona, E. Enzo, S. Giulitti, M. Cordenonsi, F. Zanconato, J. Le Digabel, M. Forcato, S. Bicciato, N. Elvassore, S. Piccolo, *Nature* **2011**, *474*, 179.

[12] M. Kuroda, H. Wada, Y. Kimura, K. Ueda, N. Kioka, *J. Cell Sci.* **2017**, *130*, 989.

[13] S. Dupont, *Exp. Cell Res.* **2016**, *343*, 42.

[14] a) M. Guvendiren, J. A. Burdick, *Nat. Commun.* **2012**, *3*, 792; b) A. R. Killaars, J. C. Grim, C. J. Walker, E. A. Hushka, T. E. Brown, K. S. Anseth, *Adv. Sci.* **2019**, *6*, 1801483; c) V. Frank, S. Kaufmann, R. Wright, P. Horn, H. Y. Yoshikawa, P. Wuchter, J. Madsen, A. L. Lewis, S. P. Armes, A. D. Ho, M. Tanaka, *Sci. Rep.* **2016**, *6*, 24264.

[15] a) M. Tanaka, M. Nakahata, P. Linke, S. Kaufmann, *Polym. J.* **2020**, *52*, 861; b) M. Hörning, M. Nakahata, P. Linke, A. Yamamoto, M. Veschgini, S. Kaufmann, Y. Takashima, A. Harada, M. Tanaka, *Sci. Rep.* **2017**, *7*, 7660; c) K. Hayashi, M. Matsuda, N. Mitake, M. Nakahata, N. Munding, A. Harada, S. Kaufmann, Y. Takashima, M. Tanaka, *ACS Appl. Polym. Mater.* **2022**, *4*, 2595.

[16] a) A. Harada, Y. Takashima, M. Nakahata, *Acc. Chem. Res.* **2014**, *47*, 2128; b) T. Kakuta, Y. Takashima, M. Nakahata, M. Otsubo, H. Yamaguchi, A. Harada, *Adv. Mater.* **2013**, *25*, 2849; c) M. Hippler, K. Weißenbruch, K. Richler, E. D. Lemma, M. Nakahata, B. Richter, C. Barner-Kowollik, Y. Takashima, A. Harada, E. Blasco, M. Wegener, M. Tanaka, M. Bastmeyer, *Sci. Adv.* **2020**, *6*, eabc2648.

[17] A. Suzuki, T. Hara, *J. Chem. Phys.* **2001**, *114*, 5012.

[18] A. Zemel, F. Rehfeldt, A. E. X. Brown, D. E. Discher, S. A. Safran, *Nat. Phys.* **2010**, *6*, 468.

[19] a) P. Atherton, B. Stutchbury, D. Jethwa, C. Ballestrem, *Exp. Cell Res.* **2016**, *343*, 21; b) D. W. Zhou, T. T. Lee, S. Weng, J. Fu, A. J. Garcia, *Mol. Biol. Cell* **2017**, *28*, 1901. c) N. Hino, T. Ichikawa, Y. Kimura, M. Matsuda, K. Ueda, N. Kioka, *J. Cell Sci.* **2019**, *132*, jcs217349.

[20] E. G. Fey, K. M. Wan, S. Penman, *J. Cell Biol.* **1984**, *98*, 1973.

[21] M. Kuroda, K. Ueda, N. Kioka, *Sci. Rep.* **2018**, *8*, 11581.

[22] a) H. Y. Yoshikawa, T. Kawano, T. Matsuda, S. Kidoaki, M. Tanaka, *J. Phys. Chem. B* **2013**, *117*, 4081; b) S. Inoue, V. Frank, M. Hörning, S. Kaufmann, H. Y. Yoshikawa, J. P. Madsen, A. L. Lewis, S. P. Armes, M. Tanaka, *Biomater. Sci.* **2015**, *3*, 1539; c) P. Linke, R. Suzuki, A. Yamamoto, M. Nakahata, M. Kengaku, T. Fujiwara, T. Ohzono, M. Tanaka, *Langmuir* **2019**, *35*, 7538.

[23] E. Sackmann, M. Tanaka, *Biophys. Rev.* **2021**, *13*, 123.

[24] H. Tanimoto, M. Sano, *Phys. Rev. Lett.* **2012**, *109*, 248110.

[25] H. Tanimoto, M. Sano, *Biophys. J.* **2014**, *106*, 16.

[26] a) J. P. Butler, I. M. Tolic-Nørrelykke, B. Fabry, J. J. Fredberg, *Am. J. Physiol. Cell Physiol.* **2002**, *282*, C595; b) T. M. Koch, S. Münster, N. Bonakdar, J. P. Butler, B. Fabry, *PLoS One* **2012**, *7*, e33476; c) N. Schierbaum, J. Rheinlaender, T. E. Schäffer, *Soft Matter* **2019**, *15*, 1721.

[27] H. Y. Yoshikawa, F. F. Rossetti, S. Kaufmann, T. Kaindl, J. Madsen, U. Engel, A. L. Lewis, S. P. Armes, M. Tanaka, *J. Am. Chem. Soc.* **2011**, *133*, 1367.

[28] a) A. S. Burk, C. Monzel, H. Y. Yoshikawa, P. Wuchter, R. Saffrich, V. Eckstein, M. Tanaka, A. D. Ho, *Sci. Rep.* **2015**, *5*, 9370; b) H. Rieger, H. Y. Yoshikawa, K. Quadt, M. A. Nielsen, C. P. Sanchez, A. Salanti, M. Tanaka, M. Lanzer, *Blood* **2015**, *125*, 383.

[29] a) T.-P. Driscoll, B.-D. Cosgrove, S.-J. Heo, Z.-E. Shurden, R.-L. Mauck, *Biophys. J.* **2015**, *108*, 2783; b) S. R. Caliari, S. L. Vega, M. Kwon, E. M. Soulas, J. A. Burdick, *Biomaterials* **2016**, *103*, 314; c) G. Nardone, J. Oliver-De La Cruz, J. Vrbsky, C. Martini, J. Pribyl, P. Skládal, M. Pesl, G. Caluori, S. Pagliari, F. Martino, Z. Maceckova, M. Hajduch, A. Sanz-Garcia, N. M. Pugno, G. B. Stokin, G. Forte, *Nat. Commun.* **2017**, *8*, 15321.

[30] J. Oliver-De La Cruz, G. Nardone, J. Vrbsky, A. Pompeiano, A. R. Perestrelo, F. Capradossi, K. Melajová, P. Filipensky, G. Forte, *Biomaterials* **2019**, *205*, 64.

[31] T. H. Cheung, T. A. Rando, *Nat. Rev. Mol. Cell Biol.* **2013**, *14*, 329.

[32] a) A. Naji, M. Eitoku, B. Favier, F. Deschaseaux, N. Rouas-Freiss, N. Suganuma, *Cell. Mol. Life Sci.* **2019**, *76*, 3323; b) J. De Boer, H. J. Wang, C. Van Blitterswijk, *Tissue Eng.* **2004**, *10*, 393.

[33] J. C. Estrada, C. Albo, A. Benguría, A. Dopazo, P. López-Romero, L. Carrera-Quintanar, E. Roche, E. P. Clemente, J. A. Enríquez, A. Bernad, E. Samper, *Cell Death Differ.* **2012**, *19*, 743.

[34] a) G. Yourek, S. M. Mccormick, J. J. Mao, G. C. Reilly, *Regen Med* **2010**, *5*, 713; b) K. Henderson, A. D. Sligar, V. P. Le, J. Lee, A. B. Baker, *Adv. Healthcare Mater.* **2017**, *6*, 1700556.

[35] D. J. Tschumperlin, F. Liu, A. M. Tager, *Curr. Opin. Rheumatol.* **2013**, *25*, 92.

[36] M. Aragona, T. Panciera, A. Manfrin, S. Giulitti, F. Michielin, N. Elvassore, S. Dupont, S. Piccolo, *Cell* **2013**, *154*, 1047.

[37] a) J. H. Hageman, M. C. Heinz, K. Kretzschmar, J. Van Der Vaart, H. Clevers, H. J. G. Snippert, *Dev. Cell* **2020**, *54*, 435; b) S. Piccolo, M. Cordenonsi, S. Dupont, *Clin. Cancer Res.* **2013**, *19*, 4925.

[38] a) J. E. Dennis, J.-P. Carbillet, A. I. Caplan, P. Charbord, *Cells Tissues Organs* **2002**, *170*, 73; b) P. Simmons, B. Torok-Storb, *Blood* **1991**, *78*, 55.

[39] a) B. Fröhlich, A. K. Dasanna, C. Lansche, J. Czajor, C. P. Sanchez, M. Cyrklaff, A. Yamamoto, A. Craig, U. S. Schwarz, M. Lanzer, M. Tanaka, *Biophys. J.* **2021**, *120*, 3315; b) L. Yu, J. Li, J. Hong, Y. Takashima, N. Fujimoto, M. Nakajima, A. Yamamoto, X. Dong, Y. Dang, Y. Hou, W. Yang, I. Minami, K. Okita, M. Tanaka, C. Luo, F. Tang, Y. Chen, C. Tang, H. Kotera, L. Liu, *Stem Cell Rep.* **2018**, *11*, 142.

[40] a) G. Sagvolden, I. Giaever, E. O. Pettersen, J. Feder, *Proc. Natl. Acad. Sci. USA* **1999**, *96*, 471; b) Z. Guttenberg, A. R. Bausch, B. Hu, R. Bruinsma, L. Moroder, E. Sackmann, *Langmuir* **2000**, *16*, 8984; c) C. M. Franz, P.-H. Puech, *Cell Mol. Bioeng.* **2008**, *1*, 289.

[41] R. Merkel, P. Nassoy, A. Leung, K. Ritchie, E. Evans, *Nature* **1999**, *397*, 50.

[42] J. Shim, E. Hagerman, B. Wu, V. Gupta, *Acta Biomater.* **2008**, *4*, 1657.

[43] B. D. Cosgrove, K. L. Mui, T. P. Driscoll, S. R. Caliari, K. D. Mehta, R. K. Assoian, J. A. Burdick, R. L. Mauck, *Nat. Mater.* **2016**, *15*, 1297.

[44] C. Yang, M. W. Tibbitt, L. Basta, K. S. Anseth, *Nat. Mater.* **2014**, *13*, 645.

[45] a) J.-A. Dahl, S. Duggal, N. Coulston, D. Millar, J. Melki, A. Shahdadfar, J. E. Brinchmann, P. Collas, *Int. J. Dev. Biol.* **2002**, *52*, 1033; b) V. Bunpetch, Z.-Y. Zhang, X. Zhang, S. Han, P. Zongyou, H. Wu, O. Hong-Wei, *Biomaterials* **2019**, *196*, 67.

[46] C. Zhang, H. Zhu, X. Ren, B. Gao, B. Cheng, S. Liu, B. Sha, Z. Li, Z. Zhang, Y. Lv, H. Wang, H. Guo, T. J. Lu, F. Xu, G. M. Genin, M. Lin, *Nat. Commun.* **2021**, *12*, 6229.

[47] E. Novoseletskaya, O. Grigorieva, P. Nimiritsky, N. Basalova, R. Eremichev, I. Milovskaya, K. Kulebyakin, M. Kulebyakina, S. Rodionov, N. Omelyanenko, A. Efimenko, *Front. Cell Dev. Biol.* **2020**, *8*, 555378.

[48] H. Hillebrandt, M. Tanaka, *J. Phys. Chem. B* **2001**, *105*, 4270.

[49] M. Nakahata, Y. Takashima, A. Harada, *Macromol. Rapid Commun.* **2016**, *37*, 86.

[50] J. R. Tse, A. J. Engler, *Curr. Protoc. Cell Biol* **2010**, *10*, 16.

[51] W. Wagner, R. E. Feldmann, A. Seckinger, M. H. Maurer, F. Wein, J. Blake, U. Krause, A. Kalenka, H. F. Bürgers, R. Saffrich, P. Wuchter, W. Kuschinsky, A. D. Ho, *Exp. Hematol.* **2006**, *34*, 536.

[52] J. Schindelin, I. Arganda-Carreras, E. Frise, V. Kaynig, M. Longair, T. Pietzsch, S. Preibisch, C. Rueden, S. Saalfeld, B. Schmid, J.-Y. Tinevez, D. J. White, V. Hartenstein, K. Eliceiri, P. Tomancak, A. Cardona, *Nat. Methods* **2012**, *9*, 676.